



NR2F2 controls malignant squamous cell carcinoma state by promoting stemness and invasion and repressing differentiation

Federico Mauri^{1,8}, Corentin Schepkens^{1,8}, Gaëlle Lapouge^{1,8}, Benjamin Drogat¹, Yura Song¹, Ievgenia Pastushenko¹, Sandrine Rorive^{2,3,4}, Jeremy Blondeau¹, Sophie Golstein¹, Yacine Bareche⁵, Marie Miglianico⁶, Erwin Nkusi¹, Milena Rozzi¹, Virginie Moers¹, Audrey Brisebarre¹, Maylis Raphaël¹, Christine Dubois¹, Justine Allard³, Benoit Durdu¹, Floriane Ribeiro¹, Christos Sotiriou⁵, Isabelle Salmon^{2,3,4}, Jalal Vakili⁶ and Cédric Blanpain^{1,7}✉

The nongenetic mechanisms required to sustain malignant tumor state are poorly understood. During the transition from benign tumors to malignant carcinoma, tumor cells need to repress differentiation and acquire invasive features. Using transcriptional profiling of cancer stem cells from benign tumors and malignant skin squamous cell carcinoma (SCC), we identified the nuclear receptor NR2F2 as uniquely expressed in malignant SCC. Using genetic gain of function and loss of function in vivo, we show that NR2F2 is essential for promoting the malignant tumor state by controlling tumor stemness and maintenance in mouse and human SCC. We demonstrate that NR2F2 promotes tumor cell proliferation, epithelial-mesenchymal transition and invasive features, while repressing tumor differentiation and immune cell infiltration by regulating a common transcriptional program in mouse and human SCCs. Altogether, we identify NR2F2 as a key regulator of malignant cancer stem cell functions that promotes tumor renewal and restricts differentiation to sustain a malignant tumor state.

The progression from benign to malignant tumors requires tumor cells to sustain their renewal capacity, impair their differentiation and remodel the extracellular matrix (ECM), allowing invasion. Genetic and nongenetic mechanisms have been proposed to regulate malignant transition. However, the nongenetic mechanisms that regulate the malignant tumor state remain poorly understood.

SCCs are very frequent cancers that arise in different body locations such as skin, oral cavity, head and neck, esophagus and lung; some are associated with poor clinical prognosis^{1,2}. Mouse skin SCCs present the same histology and a very similar mutational landscape as their human counterpart, providing an ideal model to study tumor initiation and progression^{3,4}. Carcinogen-induced skin SCCs are among the most extensively used mouse models for the study of tumorigenesis. In this model, topical application of 9,10-dimethyl-1,2-benzanthracene (DMBA), a potent mutagen, is followed by 12-*O*-tetradecanoylphorbol-13-acetate (TPA) treatment, which stimulates proliferation and inflammation. This treatment leads to the appearance of benign tumors called papillomas that keep the normal differentiation of the skin epidermis, with a proliferative layer of basal tumor cells and several layers of terminally differentiated, nonproliferative cells expressing K1/K10. Following TPA administration, a fraction (about 10–20%) of benign papillomas progress to invasive carcinomas, which lose K1/K10 expression, disrupt the basal lamina and can invade the

underlying mesenchyme giving rise to distant lymph node and lung metastases^{5,6}.

Cancer stem cells (CSCs) are a subpopulation of cells presenting long-term self-renewing capacities that can sustain tumor growth⁷. The most common assay to study CSCs consists in the transplantation of limiting dilutions of FACS-isolated tumor cells into immunodeficient mice. CSCs present a greater tumor-propagating cell capacity, leading to formation of secondary tumors upon transplantation of limiting dilutions of tumor cells and greater long-term self-renewal capacity, as assessed by serial transplantation⁸. In skin SCC, CSCs have been identified on the basis of their high level of basal integrin and CD34 expression^{9–12}. Molecular characterization of these CSCs has uncovered different transcription factors (TFs) such as SOX2, TWIST1 and PITX1 that regulate the renewal of CSCs in both benign papillomas and malignant SCC^{13–16}. The mechanisms specifically regulating malignant CSCs remain unknown.

To identify the mechanisms that regulate malignant CSCs in skin squamous tumors, we compared the transcriptional profile of CD34⁺Epcam⁺ tumor cells in well-differentiated papillomas and malignant SCC¹⁴. Among the TFs that were differentially regulated between these two populations, we found that at the protein level the nuclear receptor NR2F2 was exclusively expressed in malignant tumor cells, in contrast to other TFs such as SOX2, TWIST1 and PITX1, which were expressed in both benign and malignant skin tumors^{13–16} (Fig. 1a and Extended Data Fig. 1a,b). NR2F2, a TF of

¹Laboratory of Stem Cells and Cancer, Université Libre de Bruxelles (ULB), Brussels, Belgium. ²Centre Universitaire Inter Régional d'Expertise en Anatomie Pathologique Hospitalière (CurePath), Jumet, Belgium. ³DIAPath, Center for Microscopy and Molecular Imaging, Université Libre de Bruxelles (ULB), Gosselies, Belgium. ⁴Department of Pathology, Erasme University Hospital, Université Libre de Bruxelles (ULB), Brussels, Belgium. ⁵Breast Cancer Translational Research Laboratory, J.-C. Heuson, Institut Jules Bordet, Université Libre de Bruxelles, Brussels, Belgium. ⁶ChromaCure SA, Grandbonpré 11/5, Mont-Saint-Guibert, Belgium. ⁷WELBIO, Université Libre de Bruxelles (ULB), Bruxelles, Belgium. ⁸These authors contributed equally: Federico Mauri, Corentin Schepkens, Gaëlle Lapouge. ✉e-mail: Cedric.Blanpain@ulb.be

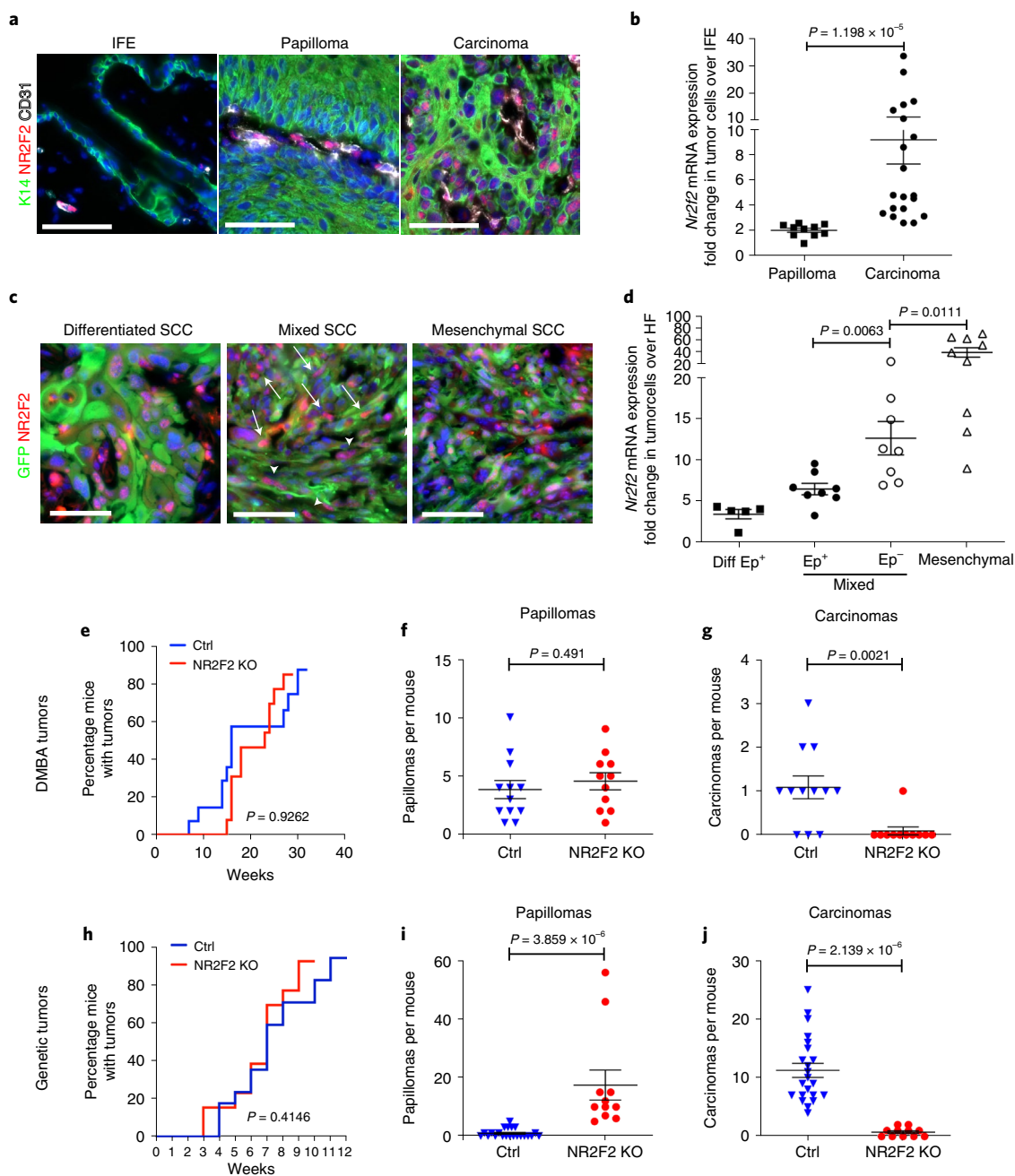


Fig. 1 | NR2F2 loss of function prevents malignant transition. **a,b**, Expression of NR2F2 in DMBA/TPA-induced tumors. Immunostaining for K14 (epithelial cells), CD31 (endothelial cells) and NR2F2 in interfollicular epidermis (IFE), benign tumors (papillomas) and malignant SCC (**a**). Representative images of at least ten independent biological replicates. qRT-PCR for *Nr2f2* in tumor cells from benign papillomas and malignant carcinomas (**b**). Messenger RNA expression is normalized to normal IFE ($n = 10$ papillomas and 20 carcinomas). **c,d**, Expression of NR2F2 in *Lgr5CreER/KRas^{G12D}/p53^{fllox}/RosaYFP*-derived SCCs. GFP⁺/Epcam⁺ population represents epithelial tumor cells, whereas GFP⁺/Epcam⁻ population represents tumor cells that underwent EMT in genetically induced skin SCCs. Immunostaining for NR2F2 and YFP in differentiated, mixed (arrowheads indicate Epcam⁺ and arrows indicate Epcam⁻ tumor cells) and mesenchymal SCCs (**c**). Representative images of at least five independent biological replicates. qRT-PCR for *NR2F2* in tumor cells isolated from differentiated, mixed (Epcam⁺ and Epcam⁻ subpopulations isolated from the same tumor) and mesenchymal genetic tumors (**d**). Expression is normalized to normal HF cells ($n = 5$ differentiated, 8 mixed and 9 mesenchymal tumors). Ep, Epcam. **e-g**, Effect of *Nr2f2* deletion in DMBA/TPA-induced tumors. Percentage of mice bearing tumors over time after DMBA/TPA treatment in wild-type (WT) and NR2F2 KO mice (**e**). Number of benign tumors (papillomas) per mouse in Ctrl and NR2F2 KO (**f**). Number of malignant SCCs per mouse in Ctrl and NR2F2 KO ($n = 12$ Ctrl and 11 NR2F2 KO mice) (**g**). **h-j**, Effect of *Nr2f2* deletion in *Lgr5CreER/KRas^{G12D}/p53^{fllox}/RosaYFP*-derived SCCs. Percentage of mice bearing tumors over time after *KRas^{G12D}* expression and *p53* deletion (**h**). Number of benign tumors (papillomas) per mouse in Ctrl and NR2F2 KO (**i**). Number of malignant SCC per mouse in Ctrl and NR2F2 KO ($n = 20$ Ctrl and 11 NR2F2 KO mice) (**j**). Scale bar, 50 μ m. Data in **b,d,f,g,i,j** are represented as mean \pm s.e.m. *P* values are calculated using a two-tailed Mann-Whitney *U*-test. In **e** and **h**, a log-rank Mantel-Cox test was used.

an orphan nuclear receptor family, is expressed during embryonic development in the mesenchymal part of various organs^{17,18}. As embryonic development proceeds, NR2F2 expression is restricted in adult tissues to some endothelial cells and the uterine mesenchyme¹⁸. In cancer, NR2F2 was initially reported to regulate tumorigenesis in a non-cell autonomous manner by regulating the tumor microenvironment, in particular neoangiogenesis. Conditional ablation of *Nr2f2* in all tissues using Rosa-CreER decreases neoangiogenesis and tumor growth upon transplantation of mouse tumor cell lines and in spontaneous mammary and pancreatic tumors^{19–21}. In addition to its expression in the tumor microenvironment, NR2F2 is expressed in various human cancers, including breast, prostate, colorectal, pancreatic and ovarian cancers^{22–24}. Conflicting studies show that NR2F2 expression in tumors can be associated with either good or poor prognosis^{23–29}. In a prostate mouse cancer model, conditional deletion of *Nr2f2* and *PTEN* in prostate epithelial cells delayed progression toward high-grade tumors; conversely *Nr2f2* overexpression in the same model accelerated tumor progression³⁰. However, the role and the mechanisms by which NR2F2 regulates malignant tumor states, tumor stemness and maintenance are currently unknown.

Here, using genetic gain of function (GOF) and loss of function in mice and human SCC, we uncover an essential role of NR2F2 in promoting a malignant tumor state and regulating tumor differentiation. Molecular profiling and in situ characterization following gain and loss of NR2F2 reveal that NR2F2 regulates different key tumor functions, promoting tumor proliferation, epithelial–mesenchymal transition (EMT), migration and stemness, while restraining differentiation and immune cell infiltration. Altogether, our study uncovers an essential role for NR2F2 in promoting the malignant tumor state and tumor stemness in SCC by regulating the balance between CSC renewal and differentiation.

Results

NR2F2 loss of function prevents malignant transition. To identify the intrinsic factors that regulate the balance between self-renewal and differentiation during the transition from benign to malignant skin squamous tumors, we performed transcriptional profiling of FACS-isolated CD34⁺ CSCs from benign and malignant carcinogen-induced skin tumors (Extended Data Fig. 1a)¹⁴. We identified *Sox2*, *Twist1*, *Pitx1*, *Hoxa9* and the orphan nuclear receptor *Nr2f2* among the most-upregulated TFs in malignant CD34⁺ CSCs compared to papilloma CD34⁺ CSCs (Extended Data Fig. 1b). SOX2, TWIST1 and PITX1, although expressed at higher levels in malignant SCCs, are also expressed in benign tumors and regulate benign tumor formation^{13–16}. To validate the results of our microarray analysis, we analyzed *Nr2f2* expression by quantitative PCR with reverse transcription (RT–qPCR) and immunofluorescence during the different stages of carcinogenesis in two different SCC models. In chemically induced (DMBA/TPA) skin SCC, we found that NR2F2 expression was absent in normal skin and benign papillomas and began to be expressed in malignant SCCs (Fig. 1a,b).

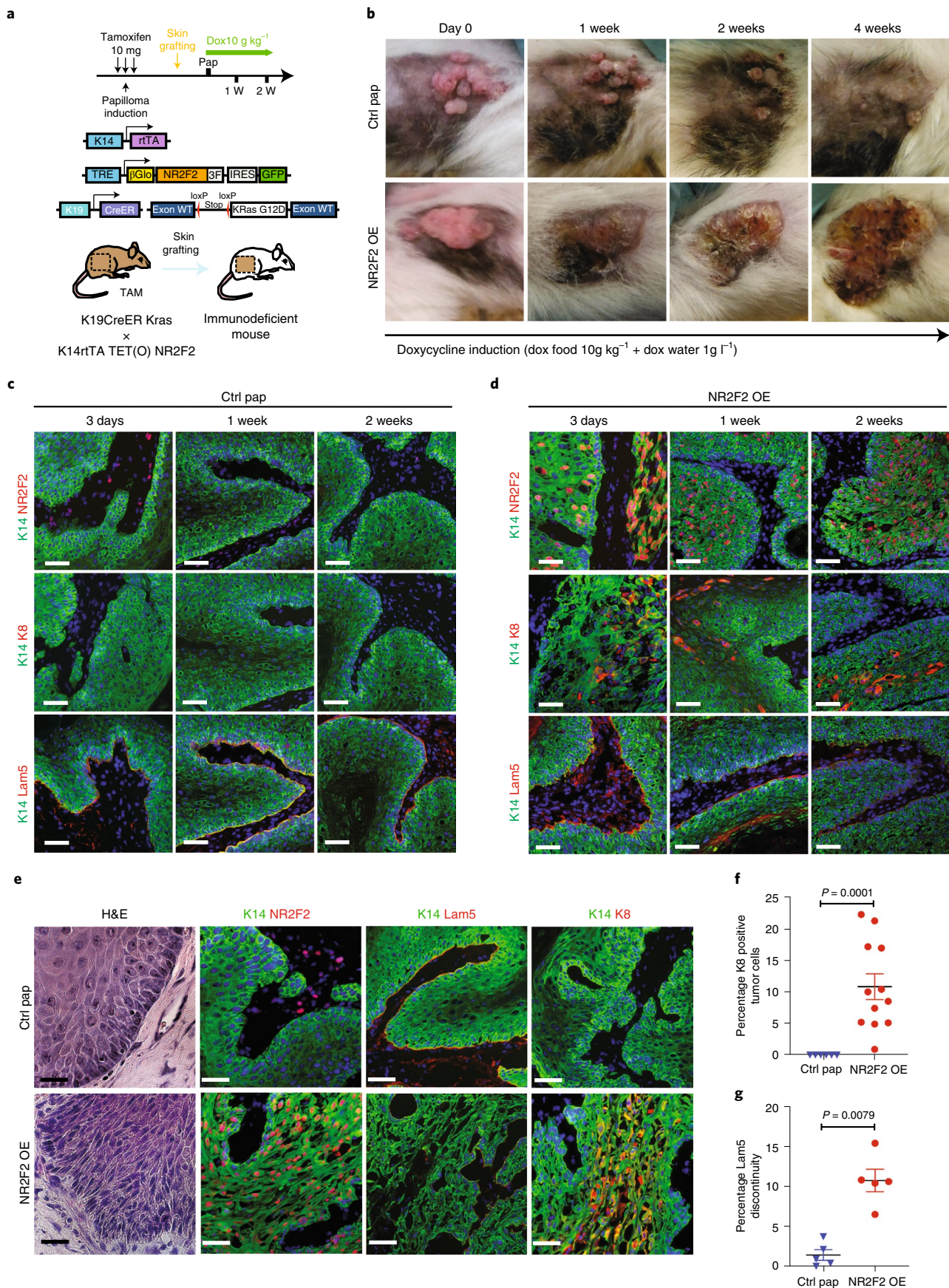
NR2F2 was preferentially expressed by CD34⁺ CSC and proliferative basal cells in DMBA/TPA SCC (Extended Data Fig. 1b–d). We then assessed NR2F2 expression in a genetic model where skin SCCs are induced by expression of *KRas*^{G12D} and *p53* deletion in hair follicle (HF) lineages using *Lgr5CreER*, which leads to the formation of skin SCC characterized by different degrees of EMT ranging from well-differentiated epithelial tumors, mixed (containing epithelial and mesenchymal tumor cells) tumors, to fully EMT tumors³¹. In these tumors, NR2F2 expression was higher and broader in SCCs that presented EMT (Fig. 1c,d and Extended Data Fig. 1f). The increase of expression of NR2F2 in invasive SCCs could be related to different factors. The somatic mutations, including those activating the Ras pathway, are found in both papillomas and SCCs³². The main genetic difference between papillomas and carcinomas is the presence of aneuploidy in SCCs, whereas no chromosomal amplifications or deletions are found in papillomas. It is thus possible that aneuploidy contributes to the expression of NR2F2. Also, differences in the tumor microenvironment may contribute to the expression of NR2F2 in malignant tumors. Consistent with this notion, NR2F2 is expressed at higher levels in tumor cells in direct contact with the stroma (Fig. 1a,c and Extended Data Fig. 1c).

To define the role of NR2F2 in malignant SCC, we first performed conditional deletion of *Nr2f2* in the skin epidermis and assessed the impact of NR2F2 loss of function in skin tumor initiation and progression. Mice homozygous for *Nr2f2* floxed alleles and carrying a *K14Cre* (referred to as NR2F2 knockout (KO)), which leads to the deletion of *Nr2f2* in all the cells of the epidermis starting during embryonic development, were born at a Mendelian ratio and did not present pathological phenotypes. Following DMBA/TPA administration, tumorigenesis developed at the same rate in NR2F2 KO and control mice, giving rise to comparable numbers of benign papillomas (Fig. 1e,f), which presented the same histology, expression of markers of differentiation (K10) and tumor angiogenesis (CD31) (Extended Data Fig. 1e). Notably, while around 20% of benign papillomas eventually progressed to malignant SCCs in control mice, the benign tumors did not progress to malignant tumors in NR2F2 KO mice even 1 year after tumor onset (Fig. 1g), demonstrating the essential role of NR2F2 in promoting malignant transition in skin SCCs. Conditional deletion of *Nr2f2* in two distinct genetic models of skin SCCs (*Lgr5CreER/KRas*^{G12D}/*p53*^{fllox}/*Nr2f2*^{fllox} and *K14CreER/KRas*^{G12D}/*p53*^{fllox}/*Nr2f2*^{fllox}), which give rise to skin tumors that invariably progress to malignant carcinomas^{33,34}, did not significantly alter tumor initiation, as the number of tumors per mice (papillomas and carcinomas) and the tumor latency were not affected by NR2F2 deletion. However, upon *Nr2f2* deletion, all tumors consisted of benign papillomas even after 12–14 weeks following tumor appearance, whereas in the absence of *Nr2f2* deletion, all tumors consisted of malignant carcinomas, showing that *Nr2f2* deletion completely prevents malignant progression (Fig. 1h–j and Extended Data Fig. 1g). Altogether, these data indicate that NR2F2 is essential for malignant progression in different mouse models of skin SCCs.

Fig. 2 | NR2F2 gain of function promotes a malignant tumor state. **a**, Strategy used to overexpress NR2F2 in papillomas after grafting in immunodeficient mice. **b**, Representative pictures of the evolution of control (Ctrl) and NR2F2 overexpression (OE) papillomas upon doxycycline administration, from day 0 (start of doxycycline treatment) until 4 weeks of treatment. Representative images of at least five independent biological replicates each in Ctrl and NR2F2 OE. **c**, Immunostaining for K14 (epithelial tumor cells), NR2F2, K8 (progression marker), Lam5 (basal lamina) at 3 d, 1 week and 2 weeks after beginning of doxycycline induction in Ctrl papillomas. Representative images of at least five independent biological replicates per condition. **d**, Immunostaining for K14 (epithelial tumor cells), NR2F2, K8 (progression marker), Lam5 (basal lamina) at 3 d, 1 week and 2 weeks after beginning of doxycycline induction in NR2F2 OE papillomas. Representative images of at least five independent biological replicates per condition. **e**, Hematoxylin and eosin (H&E) and immunostaining for K14 (tumor cells), NR2F2, Flag (ectopic NR2F2), Lam5 (basal lamina), K8 (malignant progression) in control and NR2F2 GOF papillomas 4 weeks after beginning of doxycycline induction, showing that NR2F2 OE in papillomas induces malignant progression. Representative images of at least five independent biological replicates per condition. **f**, Quantification of K8-positive tumor cells in NR2F2 OE papillomas ($n = 6$ Ctrl and 12 NR2F2 OE tumors). **g**, Quantification of basal lamina discontinuity based on laminin-5 staining in NR2F2 OE papillomas ($n = 5$ Ctrl and 5 NR2F2 OE papillomas). Scale bar, 50 μm . Data in **f** and **g** are represented as mean \pm s.e.m. *P* values are calculated using a two-tailed Mann–Whitney *U*-test.

NR2F2 gain of function promotes a malignant tumor state. As NR2F2 is required for progression of benign papillomas to malignant SCCs in vivo, we then assessed whether NR2F2 ectopic

expression in benign tumors is sufficient to alter tumor differentiation and promote malignant transition. For this purpose, we generated *K14rtTA/TRE-Nr2f2-IRES-GFP* mice allowing



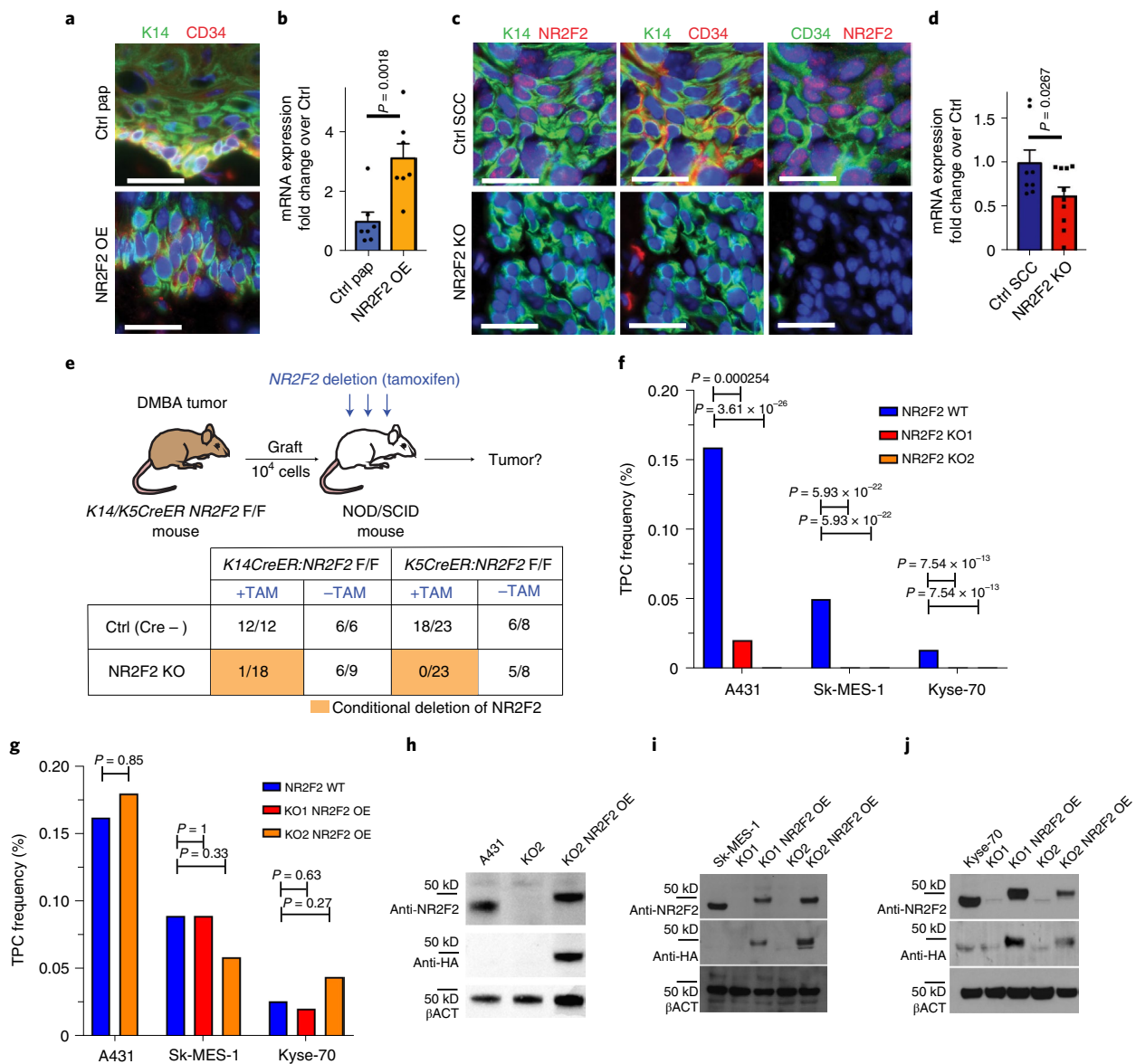


Fig. 3 | NR2F2 promotes tumor stemness in mouse and human SCC. a, Immunostaining for K14 (tumor cells) and CD34 (CSC marker) in control and NR2F2 GOF papillomas showing that NR2F2 overexpression in papillomas induces CD34 expression. Representative images of at least five independent biological replicates each for Ctrl and NR2F2 OE. **b**, qRT-PCR for CD34 in tumor cells from control and NR2F2 OE papillomas. The mRNA expression is normalized to non-induced controls ($n = 7$ Ctrl and NR2F2 OE tumors). **c**, immunostaining for K14 (tumor cells), NR2F2, CD34 (CSC marker) in Ctrl and NR2F2 KO SCC, showing that *Nr2f2* deletion in carcinomas decreases CD34 expression. Representative images of at least five independent biological replicates each for Ctrl and NR2F2 KO. **d**, qRT-PCR for CD34 in tumor cells from control and NR2F2 KO SCC. The mRNA expression is normalized to controls ($n = 8$ Ctrl and 10 NR2F2 KO tumors). **e**, Scheme of the experimental strategy and the proportion of secondary tumors following the transplantation of 10⁴ WT and NR2F2 KO mouse tumor cells, expressed as a fraction of growing secondary tumors/total of grafted points ($n = 3$ primary tumors per genotype used for the FACS isolation of tumor cells for grafting; $n = 6$ –23 tumor grafts per condition as specified). **f**, Tumor-propagating cell (TPC) frequency calculated using the extreme-limiting dilution analysis (ELDA) for A431 (skin SCC), SK-MES-1 (lung SCC) and Kyse-70 (esophagus SCC) WT and NR2F2 KO human SCC cell lines. The graph shows TPC calculated based on the ELDA exact value using $n = 3$ –5 mice per cell line and condition and two grafts per mouse. *P* value is calculated using chi-squared test. **g**, Proportion of secondary tumor formation and TPC frequency calculated by using the ELDA for A431, SK-MES-1 and Kyse-70 parental SCC cell lines and NR2F2 KO rescue clones carrying the NR2F2-3HA transgene (NR2F2 OE). *P* value is calculated using chi-squared test. The graph shows TPC calculated based on the ELDA exact value using $n = 3$ –5 mice per cell line and condition and two grafts per mouse. **h**, Western blot (WB) for NR2F2, HA tag and β -actin in parental A431 cells, NR2F2 KO or NR2F2 rescue by OE. **i**, WB for NR2F2, HA tag and β -actin in parental SK-MES-1 cells, NR2F2 KO or NR2F2 rescue by OE. **j**, WB for NR2F2, HA tag and β -actin in parental Kyse-70 cells, NR2F2 KO or NR2F2 rescue by OE. Scale bar, 50 μ m (**a**, **c**). Data in **b** and **d** are represented as mean \pm s.e.m. *P* values in **b** and **d** are calculated using a one-tailed *t*-test. Western blots are representative of two independent experiments with similar results in **h** and three independent experiments with similar results in **i** and **j**.

doxycycline-inducible overexpression of NR2F2 in all squamous epithelia. Ectopic expression of NR2F2 in adult squamous epithelia induced epidermal hypertrophy and dyskeratosis that ultimately

led to the death of the animals, presumably due to dehydration secondary to barrier dysfunction (Extended Data Fig. 2a–f). To circumvent this problem, we grafted a fragment of skin from

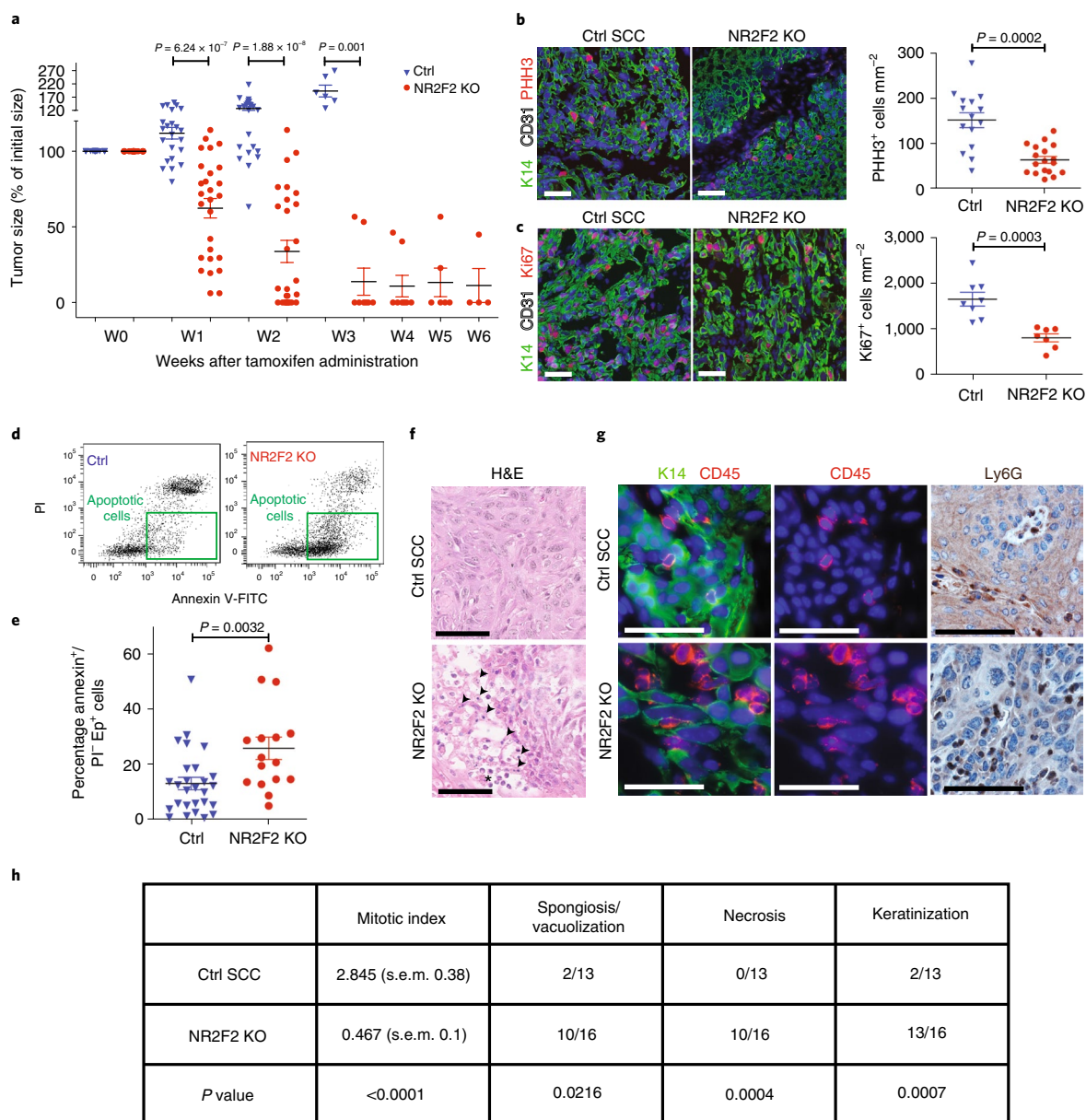


Fig. 4 | NR2F2 is essential for the maintenance of malignant SCCs. **a**, Percentage of initial tumor size over time following tamoxifen-induced *Nr2f2* deletion ($n=21$ Ctrl and 28 NR2F2 KO tumors). **b**, Immunostaining (left) for PHH3 (mitotic cells) and K14 (tumor cells) and quantification (right) of PHH3⁺ cells mm⁻² ($n=15$ Ctrl and 18 NR2F2 KO tumors). **c**, Immunostaining (left) for Ki67 (proliferating cells) and K14 (tumor cells) and quantification (right) of Ki67⁺ cells mm⁻² ($n=8$ Ctrl and 7 NR2F2 KO tumors). **d**, FACS plot of tumor cells stained with annexin V and propidium iodide (PI). **e**, Quantification of annexin V⁺/PI⁻ Epcam⁺ cells (early cell death) in Ctrl and NR2F2 KO tumors ($n=27$ Ctrl and 16 NR2F2 KO tumors). **f**, H&E staining of Ctrl and NR2F2 KO SCC. NR2F2 KO tumors display necrotic areas with picnotic nuclei (arrowheads) and polymorphonuclear cells recruitment (asterisk). **g**, Immunostaining for CD45 (immune cells) and K14 (tumor cells) and immunohistochemistry (IHC) for Ly6G (neutrophils) showing immune cell infiltration of the tumor following *Nr2f2* deletion. Representative images of at least five independent biological replicates per condition. **h**, Summary table of the histopathological analysis of Ctrl and NR2F2 KO tumors, considering mitotic index (per high-power field), necrosis, spongiosis/vacuolization and keratinization ($n=13$ Ctrl and 16 NR2F2 KO tumors). Scale bar, 50 μ m. Data in **a–c, e** are represented as mean \pm s.e.m. *P* values are calculated using a two-tailed Mann–Whitney *U*-test. For **h**, we used a two-tailed Mann–Whitney *U*-test for the mitotic index and two-tailed Fisher’s exact test in all other cases.

K19CreER/KRas^{G12D}/K14rtTA/TRE-Nr2f2-IRES-GFP mice onto the back of immunodeficient mice, where the formation of benign papillomas is induced after tamoxifen administration^{33,34} (Fig. 2a). *KRas^{G12D}* expression without *p53* deletion in this mouse model induces formation of benign papillomas that do not progress spontaneously to malignant SCC^{10,33,34}. When papillomas started developing, we induced NR2F2 ectopic expression in papilloma and its adjacent skin by administrating doxycycline (Fig. 2a). NR2F2

overexpression in papillomas led progressively to the disruption of normal differentiation and the induction of features of malignant progression, characterized by changes in the shape and adhesion of tumor cells, the expression of K8, a marker of malignant progression in skin SCC³⁵ and ultimately the discontinuation of the basal lamina, a key feature of malignant progression (Fig. 2b–g). At 30–40 days following NR2F2 overexpression, the grafted tumors had increased in size and presented macroscopic features of SCC,

sometimes with ulceration of tumors (Fig. 2b), which required terminating the experiments.

NR2F2 promotes tumor stemness in mouse and human SCC. As NR2F2 is preferentially expressed by malignant CD34⁺ CSCs, we assessed the impact of NR2F2 GOF and loss of function on CD34⁺ CSCs. Overexpression of NR2F2 in papillomas caused expansion of CD34-expressing tumor cells and CD34 levels of expression in tumor cells (Fig. 3a,b). Conversely, conditional deletion of NR2F2 in malignant SCC drastically reduced expression of CD34 in tumor cells (Fig. 3c,d). Because CD34⁺ CSCs present increased tumor-propagating cell frequency and long-term self-renewal capacities upon serial transplantation into immunodeficient mice (functional properties referred to as tumor stemness^{10,11}), we tested whether *Nr2f2* deletion in malignant SCC impacts mouse and human tumor-propagating capacity. To evaluate the role of NR2F2 in mouse tumor stemness, we isolated tumor cells from chemically induced primary SCCs from *K5CreER/Nr2f2^{lox}* or *K14CreER/Nr2f2^{lox}* mice and transplanted 10⁴ cells subcutaneously into NOD/SCID immunodeficient mice, a number of cells that gives rise to secondary tumors in almost 100% of cases¹⁰. Two days after transplantation, we administered tamoxifen to recipient mice to induce NR2F2 deletion and examined the impact on frequency of secondary tumor formation (Fig. 3e). Tamoxifen treatment of mice carrying *Nr2f2* floxed alleles and inducible CreER completely abrogated the ability of tumor cells to form secondary tumors, whereas tumor-propagating capacity was unaffected in control mice, demonstrating the essential role of NR2F2 in controlling tumor propagation of malignant mouse SCC.

To assess whether NR2F2 is also essential for tumor stemness in human cancers, we used the CRISPR-Cas9 system to induce NR2F2 deletion in human SCC cell lines of various origins including skin (A431), lung (SK-MES-1) and esophagus (Kyse-70) SCC and assessed their tumor-propagating capacity upon grafting of limiting dilutions of tumor cells into immunodeficient mice. The validation of KO clones was assessed by PCR, sequencing and western blot (Fig. 3h–j). The tumor-propagating capacity of human SCC cells was strongly reduced (A431) or completely abolished (SK-MES-1 and Kyse-70) upon NR2F2 KO (Fig. 3f and Extended Data Fig. 3a). Hemagglutinin (HA)-tagged NR2F2 re-expression using lentiviral transduction of SK-MES-1, A431 and Kyse-70 NR2F2 KO clones rescued tumor-propagating capacity to the same levels as parental cell lines (Fig. 3g–j and Extended Data Fig. 3b).

Overall, these data demonstrate that NR2F2 is essential for tumor propagation/stemness in mouse and human SCC from different origins.

NR2F2 is essential for the maintenance of malignant SCCs. To define the role of NR2F2 in the maintenance of the malignant tumor state, we assessed the impact of *Nr2f2* acute deletion in pre-existing mouse skin SCC. For this purpose, we generated *K5CreER/Nr2f2^{lox}*

(NR2F2 inducible KO) mice and treated them with DMBA/TPA to induce SCC formation. Once macroscopic malignant tumors appeared, we administered tamoxifen to induce acute *Nr2f2* deletion in skin SCC. Tamoxifen administration in mice that did not express CreER had no effect on tumor growth. However, upon *Nr2f2* deletion in *K5CreER/Nr2f2^{lox}* mice, tumors rapidly shrunk, disappearing completely and permanently (Fig. 4a). The rare tumors that did not completely disappear were formed almost exclusively of keratinized or fibrotic tissue, with no residual tumor cells (Extended Data Fig. 4a,b). In the few cases where tumors relapsed after tamoxifen induction, NR2F2 was expressed in tumor cells (Extended Data Fig. 4c,d), showing that tumor relapse was mediated by tumor cells that escaped *Nr2f2* deletion.

To determine the cellular mechanisms by which NR2F2 controls the maintenance of malignant tumor states, we assessed cell proliferation, cell death and tumor histology 5 days (5 d) after tamoxifen administration in mice presenting SCC. Upon *Nr2f2* deletion, proliferation of tumor cells was decreased as shown by the reduction of phosphohistone H3 (PHH3) and Ki67-positive cells (Fig. 4b,c). In addition, *Nr2f2* deletion in malignant SCC promoted cell death as shown by the increase of annexin V-positive/propidium iodide-negative cells after tamoxifen administration (Fig. 4d,e). Histological analysis of these tumors revealed the presence of necrotic areas and immune cell infiltration mostly composed of neutrophils (Fig. 4f,g). A detailed histopathological analysis confirmed the presence of extensive cell vacuolization, necrosis, keratinization and reduction of the mitotic index in NR2F2 KO tumors (Fig. 4h).

Altogether, these data reveal that NR2F2 controls tumor maintenance by promoting tumor cell proliferation, restricting tumor cell death and immune cell infiltration.

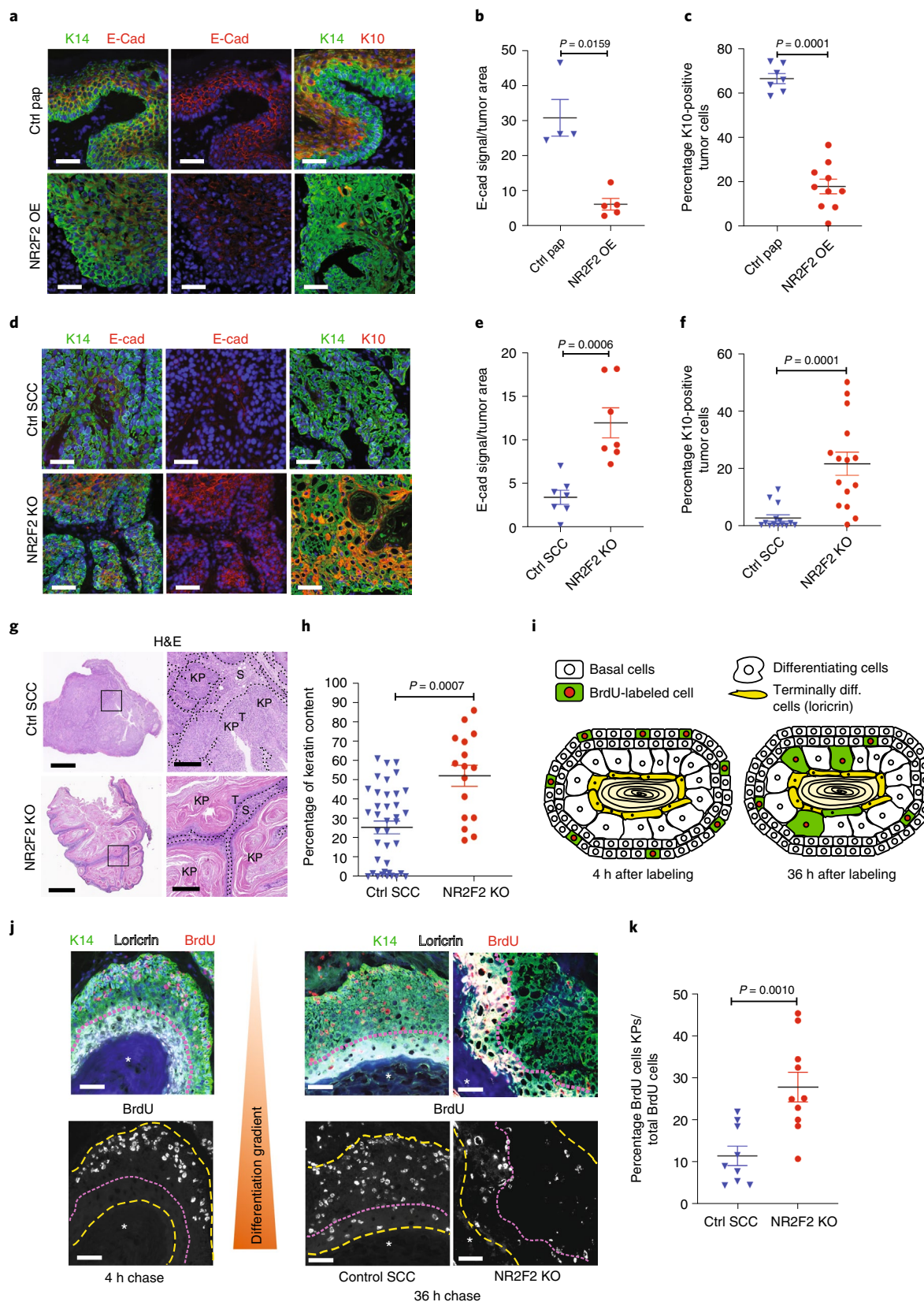
***Nr2f2* deletion promotes tumor differentiation.** The progression of benign papillomas to malignant carcinomas is associated with a block of differentiation and the disappearance of differentiation markers such as K1/K10. As *Nr2f2* deletion blocks malignant transition (Fig. 1e–j), while its ectopic expression in benign papillomas promotes malignant features (Fig. 2b–g), we assessed whether NR2F2 controls tumor differentiation. To this end, we examined the impact of NR2F2 overexpression on the differentiation of skin papillomas. NR2F2 overexpression in papillomas induced a reduction of E-cadherin and K10 expression (Fig. 5a–c and Extended Data Fig. 4e,f), indicating that NR2F2 blocks the differentiation of benign tumor cells. We then determined whether NR2F2 prevents tumor differentiation in malignant SCC. At 5 d after *Nr2f2* deletion in malignant SCCs, NR2F2 KO tumors already presented a strong increase in E-cadherin and K10 expression (Fig. 5d–f). The increase in tumor differentiation was also apparent by the extended presence of keratinized areas in the center of tumors 5 d after *Nr2f2* deletion (Fig. 5g,h). These data show that NR2F2 restricts tumor differentiation in malignant SCC.

Fig. 5 | *Nr2f2* deletion promotes CSC differentiation. a–c, Evaluation of the impact of NR2F2 ectopic expression on papilloma differentiation.

Immunostaining for K14 (tumor cells), E-Cad and K10 in Ctrl and NR2F2 OE in papilloma (a). Representative images of minimum four independent biological replicates each for Ctrl and NR2F2 OE. Quantification of E-Cad signal in Ctrl and NR2F2 OE papillomas ($n = 4$ Ctrl and 5 NR2F2 OE papillomas) (b). Quantification of K10 expression in Ctrl and NR2F2 OE papillomas ($n = 7$ Ctrl and 10 NR2F2 OE papillomas) (c). d–f, Consequences of *Nr2f2* deletion on carcinoma differentiation. Immunostaining for K14 (tumor cells), E-Cad and K10 in Ctrl and NR2F2 KO SCC (d). Representative images of a minimum of seven independent biological replicates. Quantification of E-Cad signal in Ctrl and NR2F2 KO carcinomas ($n = 7$ Ctrl and 7 NR2F2 KO SCC) (e). Quantification of K10 expression in Ctrl and NR2F2 KO carcinomas ($n = 14$ Ctrl and 15 NR2F2 KO SCC) (f). g, H&E staining showing the extensive keratinization of NR2F2 KO tumors compared to Ctrl. T, tumor cells; S, stroma; KP, Keratin Pearl. Representative images of a minimum of 16 independent biological replicates each for NR2F2 KO and Ctrl tumors. h, Quantification of keratinized areas within tumors ($n = 38$ Ctrl and 16 NR2F2 KO areas). i, Scheme of BrdU pulse-chase experiment following *Nr2f2* deletion. j, Representative images of immunostaining for BrdU-labeled cells, K14 (tumor cells) and Loricrin (terminally differentiated area) after 4 h (left) and 36 h (right) of chase in control and NR2F2 KO tumors. Asterisk indicates terminally differentiated area. k, Quantification of BrdU⁺ tumor cells within the terminally differentiated area ($n = 9$ Ctrl and 10 NR2F2 KO tumors). Scale bars, 50 μ m; 1 mm (g, left), 250 μ m (g, right). Data in b,c,e,f,h,k are represented as mean \pm s.e.m. *P* values are calculated using a two-tailed Mann–Whitney *U*-test.

To substantiate the notion that NR2F2 restricts tumor differentiation, we performed short-term lineage tracing using 5-bromodeoxyuridine (BrdU) pulse-chase experiments to trace the fate of proliferating tumor cells in this model. A pulse of BrdU

administration labeled proliferative cells and was followed by a chase of 36 h, allowing differentiating tumor cells to move toward the differentiated keratin pearls (Loricrin positive, Fig. 5i). NR2F2 KO tumors displayed a significant increase in the proportion



of BrdU/Loricrin double-positive differentiated tumor cells (Fig. 5j,k), showing that *Nr2f2* deletion dramatically accelerated tumor differentiation.

NR2F2 target genes regulate distinct tumor functions. To gain further insights into the molecular mechanism by which NR2F2 regulates tumor maintenance in SCC, we performed transcriptional profiling of FACS-isolated tumor cells 7 d after NR2F2 overexpression in benign papillomas, when phenotypic changes become fully penetrant and 5 d after *Nr2f2* deletion in malignant SCC, when NR2F2 protein is completely lost (Fig. 2c,d). Unbiased Gene Ontology analysis of genes downregulated following *Nr2f2* deletion in malignant mouse skin tumors and upregulated in benign papillomas upon NR2F2 overexpression showed that these genes are enriched for factors involved in ECM remodeling, collagen fiber organization, cell migration, EMT and angiogenesis (Fig. 6a). Genes upregulated following *Nr2f2* deletion in malignant tumors showed significant enrichment for genes controlling DNA replication and repair, differentiation and immune cell chemotaxis (Extended Data Fig. 5a,b). The common genes that were downregulated upon *Nr2f2* deletion in malignant tumor cells and upregulated upon NR2F2 overexpression in benign papillomas included many ECM components and ECM remodeling factors (for example *Mmp19*, *Nid1* and *Loxl1/2*), adhesion molecules (for example *Itgβ3* and *Vcam1*), coagulation factors and cytokines (for example *Plat1*, *Il1b* and *Il6*), EMT markers (for example *Pdfrb*, *Vim*, *Krt8*, *Zeb1/2* and *Prrx1*), signaling molecules (for example *Wnt5a*, *Fstl1*) and CSC markers (for example *Aldh1a3*, *Nrp1* and *Flt1*)^{9,36,37} (Fig. 6b,c). In addition to the common molecular signature between papillomas and SCCs, other genes were regulated only in SCCs, including EMT associated factors (for example *TGF-β2/3* and *Runx1/2*), ECM factors (for example *Mmp2* and *Fn1*), secreted factors involved in the regulation of lymphangiogenesis, angiogenesis and tumor progression (for example *Vegfc*, *Angptl1* and *Spp1*) and surface molecules expressed during tumor progression (for example *Alcam*) (Fig. 6c).

To validate our transcriptional analysis, we assessed expression of differentially regulated genes at the protein level following *Nr2f2* deletion in skin SCC. Integrinβ3/CD61 (which has been implicated as a CSC marker in breast cancer and identified as one of the markers expressed during EMT transition states in skin SCC^{38,39}), the adhesion molecule Alcam (which has been proposed as a marker of tumor progression and CSC^{40,41}) and the noncanonical Wnt ligand Wnt5a (which promotes tumor aggressiveness⁴²) were all strongly decreased following *Nr2f2* deletion in SCC (Fig. 6d).

Nr2f2 overexpression in papillomas led to upregulation of several EMT genes such as *Zeb1/2*, *Twist1*, *Vim*, *Fn1* and *Col3a1* (Fig. 6e–g) and expression of K8, a marker of carcinoma progression⁴³ (Fig. 2c–f). Conversely, *Nr2f2* deletion in carcinomas decreased expression of K8 (Extended Data Fig. 5c,d). These data suggest that NR2F2 acts upstream of canonical EMT TFs to promote tumor invasion. During cancer progression, tumor cells need to remodel the ECM allowing tumor invasion. In accordance with our transcriptional profiling, *Nr2f2* deletion in SCC decreased collagen fiber deposition, as shown by Masson's staining (Fig. 6h). Expression of Fibronectin 1 and MMP19, which promotes ECM degradation, were both substantially decreased after NR2F2 deletion (Fig. 6h). Overall, these data show that NR2F2 acts upstream of key EMT regulators and promotes tumor progression by regulating ECM remodeling. To assess the functional relevance of these findings, we assessed whether *Nr2f2* deletion decreased metastasis. To this end, we performed tail vein injection of mouse and human tumor cells after *Nr2f2* deletion. Notably, *Nr2f2* deletion dramatically decreased lung metastasis in both mouse and human SCCs (Fig. 6i,j).

Altogether, our molecular profiling and in situ characterization following NR2F2 GOF and loss of function show that NR2F2 controls a transcriptional program that regulates different tumor functions, including tumor stemness, EMT and ECM remodeling, promoting a malignant tumor state and metastasis.

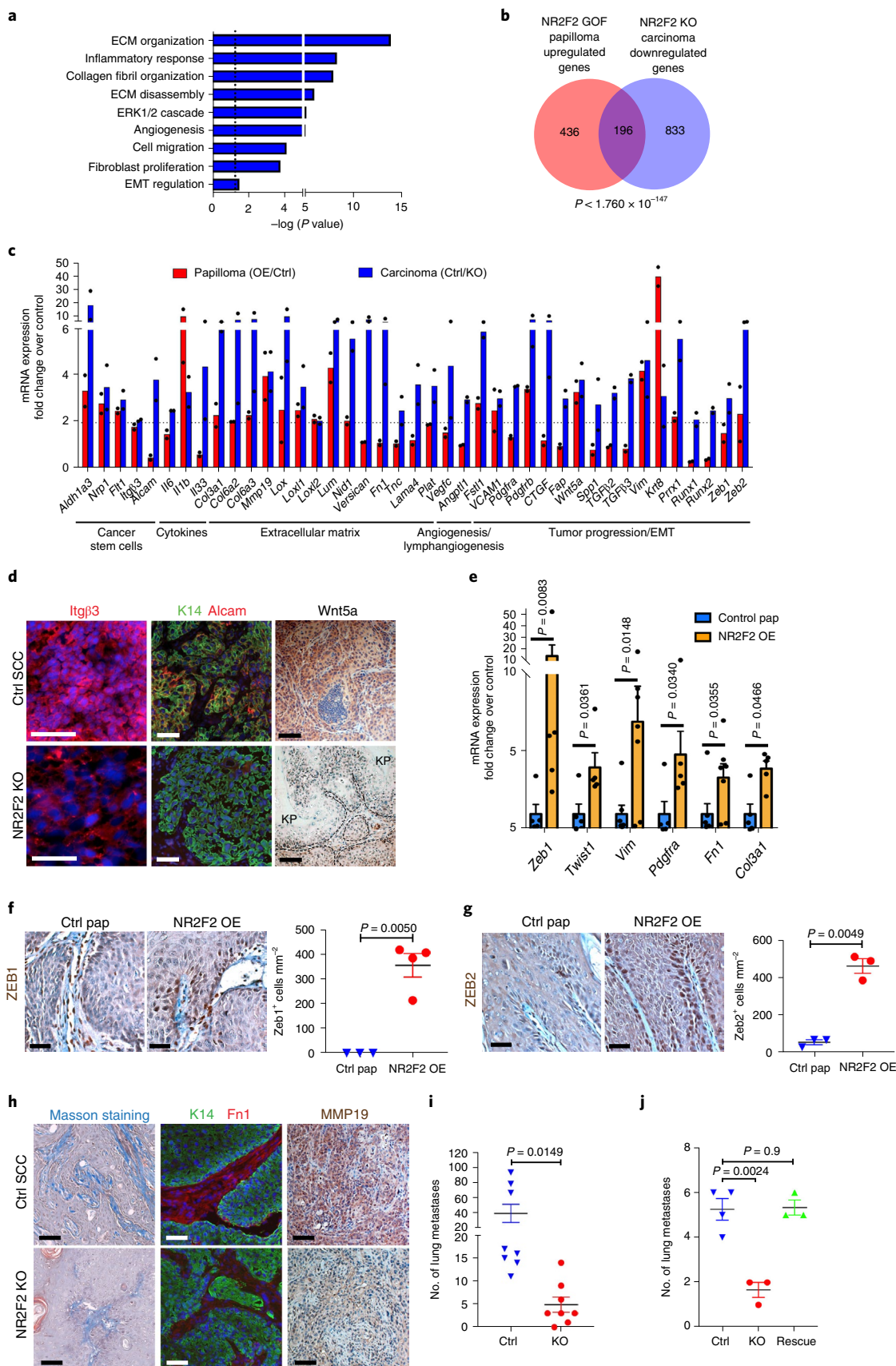
NR2F2 functions in human SCCs. To assess the human relevance of our findings, we assessed NR2F2 expression in human SCC (hSCC) from different anatomical locations. Similar to what we found in mouse SCC, NR2F2 was not expressed in normal human skin and pre-malignant lesions such as actinic keratosis and was expressed in a heterogeneous manner in skin, head and neck, lung and esophageal SCC (Fig. 7a).

To determine whether the level of NR2F2 expression was associated with clinical outcome in human cancers, we analyzed the correlation between NR2F2 expression and disease-free survival in human SCC. In cervix SCC, NR2F2 expression was very heterogeneous across the different patients and the level of NR2F2 expression correlated with poor disease-free survival (Fig. 7b,c). To further assess the clinical relevance of our findings, we evaluated the effect of administration of a small-molecule inhibitor targeting NR2F2 on A431, a human skin SCC cell line, in vitro and in vivo. Very recently, a small-molecule inhibitor targeting NR2F2 and its effect in inhibiting the growth of prostate cancer cell lines was described⁴⁴. Similarly to what has been reported in that study⁴⁴, CIA1 inhibited the growth of human A431 human skin SCC cells in vitro, but did not inhibit

Fig. 6 | NR2F2 target genes regulate distinct tumor functions. **a**, Gene Ontology analysis of genes that are downregulated in NR2F2 KO carcinomas and upregulated in NR2F2 GOF papillomas, showing categories that are significantly enriched (dotted line $P=0,05$). P value is calculated according to the Benjamini–Hochberg method for multiple hypothesis testing. **b**, Venn diagram showing the overlap between genes upregulated in NR2F2 OE papillomas and downregulated in NR2F2 KO carcinomas (fold change >2 OE/Ctrl in papillomas; Ctrl/KO in carcinomas; P value is calculated using two-sided hypergeometric test). **c**, Bar graph representation of selected genes that are upregulated in NR2F2 OE papillomas and downregulated in NR2F2 KO tumors, grouped by their respective function (fold change OE/Ctrl in papillomas; Ctrl/KO in carcinomas; $n=2$ Ctrl and NR2F2 OE papillomas; $n=2$ Ctrl and NR2F2 KO carcinomas; independent biological replicates). **d**, Immunostaining validation of selected genes from the microarray analysis in SCC following *Nr2f2* deletion. Immunostaining for Itgβ3, K14 (tumor cells) and Alcam and IHC for Wnt5a in WT and NR2F2 KO tumors. Representative images of minimum five independent biological replicates each per condition. KP, Keratin Pearls. **e**, qRT-PCR for selected EMT markers in tumor cells from NR2F2 OE papillomas. The mRNA expression is normalized to non-induced controls ($n=5$ Ctrl and NR2F2 OE papillomas). **f,g**, Upregulation of Zeb1 and Zeb2 in NR2F2 OE papillomas. Immunohistochemistry of Zeb1 and Zeb2 in Ctrl and NR2F2 OE ($n=3$ and 4 papillomas, respectively) (**f**). IHC of Zeb2 and quantification of expression in Ctrl and NR2F2 OE ($n=3$ and 4 papillomas, respectively) (**g**). **h**, Staining for collagen fibers (Masson staining), immunofluorescence for K14 (tumor cells) and Fibronectin 1 and immunohistochemistry for MMP19 in Ctrl and NR2F2 KO SCC. Representative images of minimum five independent biological replicates each per condition. **i**, Quantification of the number of lung metastasis 1 month after intravenous injection of 5×10^4 K5CreER *Nr2f2*^{lox} cells and subsequent administration of tamoxifen (KO) or no treatment (Ctrl); $n=3$ matched replicates of KO/Ctrl with cells isolated from three primary tumors independently. **j**, Quantification of the number of lung metastasis 1 month after intravenous injection of SK-MES-1 cells (Ctrl), NR2F2 KO cells (KO) and the respective NR2F2 rescue cell line (Rescue); $n=4$ independent experiments for SK-MES-1, 3 for NR2F2 KO and Rescue. Scale bar, 50 μm. Data in **e–g,i,j** are represented as mean \pm s.e.m. P values are calculated using a two-tailed Welch's t -test for **e–g**, two-way analysis of variance (ANOVA) for **i** and unpaired t -test for **j**.

the growth of other human cancer cell lines that do not express *NR2F2* (Extended Data Fig. 6a,b). In addition, CIA1 treatment inhibited the tumor-propagating capacity of human A431 (Fig. 7d

and Extended Data Fig. 6c), as well as the growth of established human A431 tumors grafted into immunodeficient mice (Fig. 7e). Histological analysis of treated tumors showed that administration



of the NR2F2 antagonist inhibited tumor cell proliferation, ECM deposition and tumor neoangiogenesis and promoted tumor cell death, tumor differentiation and immune cell infiltration, mimicking the functional consequences of NR2F2 deletion in mouse skin SCC (Fig. 7f–k and Extended Data Fig. 6d). These data provide the proof of principle demonstrating that targeting NR2F2 efficiently inhibits growth of human SCCs.

To assess whether NR2F2 controls similar functions across different human tumors, we generated two independent doxycycline-inducible short-hairpin (sh)RNA lines against NR2F2 in A431 hSCC cells (NR2F2 KD1 and KD2; Extended Data Fig. 7a), allowing us to perform an acute knockdown (KD) of NR2F2 in tumor cells similarly as in mouse experiments. Acute shRNA KD of NR2F2 decreased proliferation of A431 cells as well as their ability to grow as a tumor sphere, consistent with the importance of NR2F2 in regulating proliferation and stemness (Fig. 8a and Extended Data Fig. 7b). Assays measuring aldehyde dehydrogenase (ALDH) activity such as AldeRed or AldeFluor, have been widely used to characterize CSC-like cells in different tumor models^{45,46}. NR2F2 shRNA KD decreased the proportion of AldeRed-positive cells in both NR2F2 KD cell lines, supporting the notion that NR2F2 controls tumor stemness in mouse and human SCCs (Fig. 8b). NR2F2 shRNA KD decreased cell migration in wound scratch assays in both NR2F2 KD A431 cell lines (Fig. 8c and Extended Data Fig. 7c,d). Finally, we tested whether NR2F2 loss of function promotes tumor differentiation in the A431 cell line. To this end, we cultured these cells in high calcium, which stimulates differentiation of squamous epithelial cells^{47,48} and induced NR2F2 shRNA KD by administering doxycycline. NR2F2 shRNA KD stimulated squamous differentiation as shown by upregulation of terminal differentiation markers such as KRT10 and IVL, as well as TFs mediating squamous differentiation such as HES1, OVOL1 and GRHL1 (Fig. 8d). Altogether these data show that acute NR2F2 shRNA KD in human SCC cell lines recapitulates key features of the phenotype found upon NR2F2 deletion in mouse SCC, including decrease in proliferation, stemness, migration and increase in differentiation.

To assess the transcriptional program controlled by NR2F2 in human skin SCC tumors, we performed RNA-seq of wild-type and NR2F2 shRNA KD1 and KD2 cells 72 h following doxycycline addition, which allows the complete disappearance of NR2F2 at the protein level (Extended Data Fig. 7a). We analyzed genes expressed at more than 5 reads per million that were up- and downregulated by >1.5-fold in biological duplicates. NR2F2 KD induced downregulation of a similar transcriptional program between the two NR2F2 KD cell lines (45% overlap among downregulated genes and 24%

overlap among upregulated genes). The slight difference in strength of phenotype and gene expression observed between the two different SCC cell lines is likely to come from the distinct puromycin selection history that these two cell lines had experienced and the basal level and fold change of NR2F2 downregulation following shRNA KD (higher in cell line KD1).

A lower but nevertheless highly significant fraction of these downregulated and upregulated genes was commonly deregulated in mouse SCCs following acute NR2F2 deletion, with a greater overlap between mouse skin SCC and NR2F2 KD2 cell line (12% of downregulated mouse genes) than between mouse skin SCC and NR2F2 KD1 cell line (7% of downregulated mouse genes) (Fig. 8e,f). The common deregulated genes between mouse SCC and human skin SCC comprised many ECM molecules (COL3A1, COL5A1, COL5A2, COL8A2, LOX and MATN2), stemness markers (ALDH3A1), adhesion molecules (CLDN1 and MUC1), TFs (ELF3, FOSL2, NR2F2, NPAS2, HOXD9 and POU6F1), long-noncoding RNA (MALAT1), regulators of metabolism (H6PD), signaling molecules (TGFβ2, S100A9, ARHGEF25 and NEBL) promoting tumor progression, migration and invasion (Fig. 8g). Similarly, upregulated genes between mouse and human SCC comprised genes involving recruitment of immune/inflammatory cells (CXCL11) and squamous differentiation (GRHL3) (Fig. 8h and Extended Data Fig. 7e). Altogether, these data demonstrate that NR2F2 controls a common and tumor-specific transcriptional program, which is conserved between mouse and human skin SCCs.

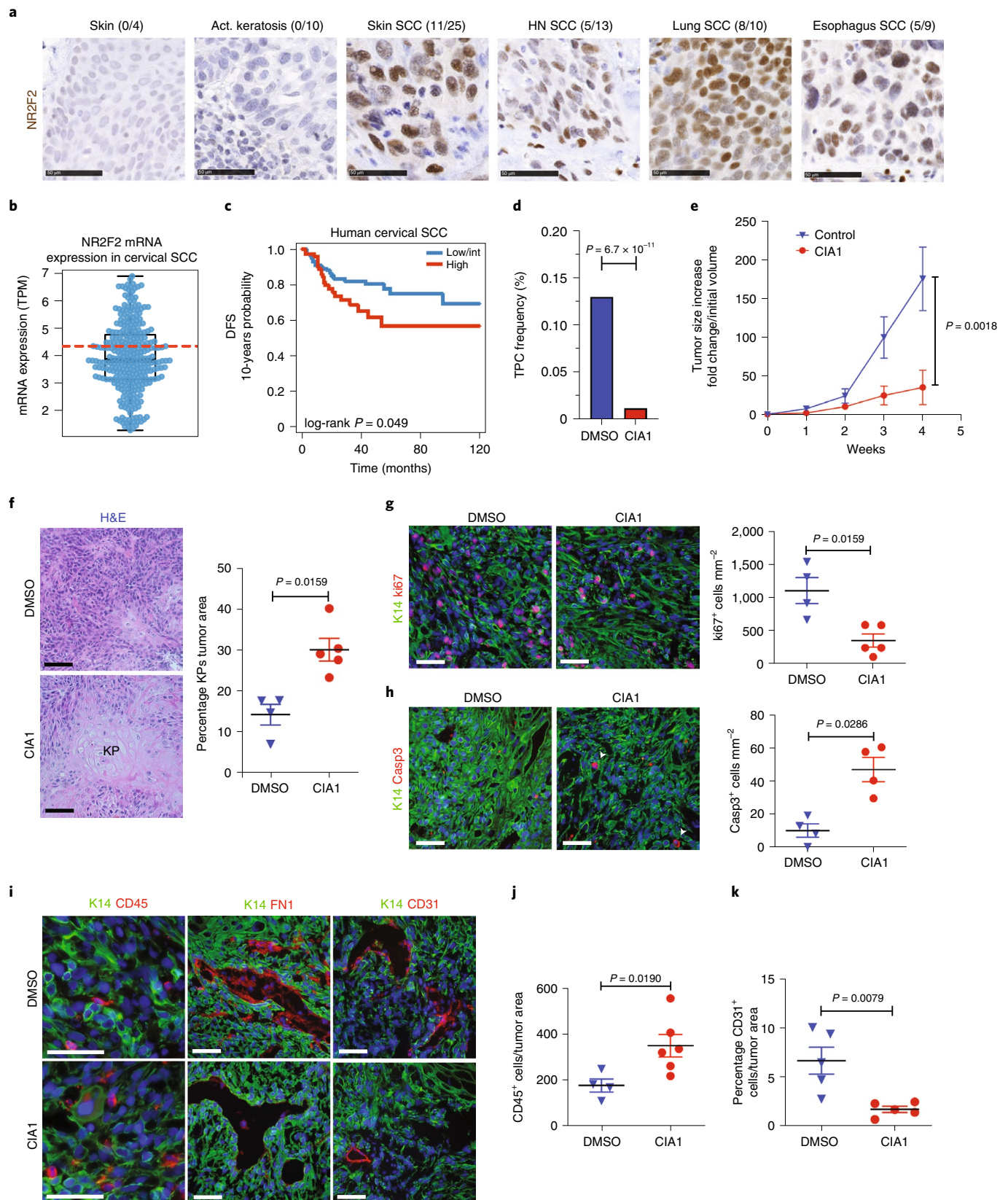
To identify direct versus indirect NR2F2 target genes, we performed NR2F2 ChIP-seq in vitro in duplicate biological samples with NR2F2 GOF A431 cells bearing an N-terminal 3HA tag (Extended Data Fig. 7f). This ChIP-seq uncovered about 2,635 NR2F2 binding sites found in duplicate samples (Fig. 8i). Motif discovery analysis retrieved NR2F2 canonical binding sites (AAAGGTCA) as the most highly significant enriched TF motifs present in more than 80% of the peaks ($P = 10 \times 10^{-193}$) (Fig. 8j). In addition, the enhancers bound by NR2F2 presented enrichment for AP1 and RUNX TF motifs, which are TFs that are well known to regulate skin cancer development and cancer^{49,50}, suggesting that NR2F2 regulates gene expression together with AP1 and RUNX (Fig. 8j). About 10% of the genes downregulated and upregulated following acute KD of NR2F2 in the A431 human skin SCC cell line NR2F2 KD1 but also in the KD2 were directly overlapping with the ChIP-seq identified peaks, demonstrating that NR2F2 is directly regulating a significant fraction of transcriptional targets identified upon loss of function (Fig. 8k and Extended Data Fig. 7g,h). Notably, NR2F2 directly regulated expression of key TFs that promote tumorigenesis in different cancers, including FOSL2, a member of AP1, NPAS2, ZBTB20 (in all

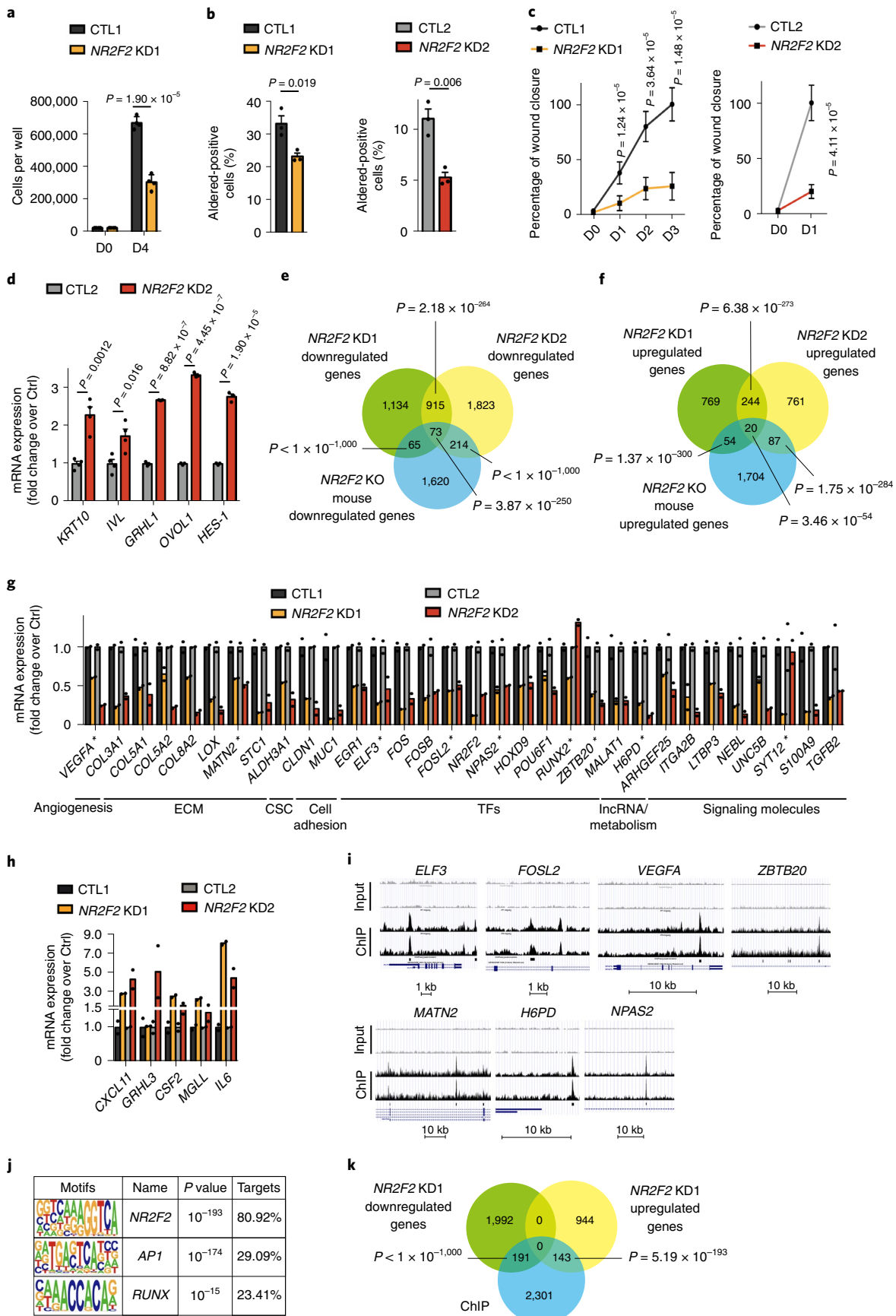
Fig. 7 | Targeting NR2F2 function in human SCCs. **a**, IHC for NR2F2 in human skin, benign lesions (actinic keratosis) and various SCC types. Above each panel the fraction of positive samples is indicated. Scale bar, 50 μm. Representative images from independent replicates as indicated above each panel ($n = 4$ skin, 10 actinic keratosis, 25 skin SCC, 13 HN SCC, 10 lung SCC and 9 esophagus SCC). HN, Head and Neck. **b**, Box plot of NR2F2 mRNA expression measured in transcripts per million in biopsies of human cervical SCC. Boundaries of the box indicate the first and third quartiles of the NR2F2 mRNA expression value. The bold black horizontal line indicates the median, the two external horizontal black lines show minimum and maximum values and the bold dotted red line represents the top tertile. The dots represent all data points ($n = 304$ biologically independent samples). **c**, Disease Free Survival (DFS) of patients with cervical SCC stratified by the level of NR2F2 expression (top-tertile cutoff point) ($P = \log$ -rank Mantel–Cox test); $n = 304$ biologically independent samples described in **b**. **d, e**, Targeting NR2F2 with small-molecule inhibitor in hSCC. TPC frequency calculated by ELDA of human skin A431 cells following CIA1 treatment (**d**). P value is calculated using chi-squared test. The graph shows TPC calculated based on the ELDA exact value using per condition; $n = 4$ –6 mice for the dimethylsulfoxide (DMSO) treatment and $n = 5$ –6 mice for the CIA1 treatment and two grafts per mouse. Increase in grafted A431 tumor volume compared to initial volume at the beginning of CIA1 treatment (**e**). P value is calculated using mixed-effect ANOVA ($n = 7$ tumors for DMSO control; 10 for CIA1 treatment). **f–k**, Histology of CIA1 treated xenograft tumors. H&E of Ctrl and CIA1-treated tumors displaying increased presence of Keratin Pearls (KP) and quantification of KP per tumor area ($n = 4$ DMSO control and 5 CIA1-treated tumors) (**f**). Immunostaining (left) for Ki67 (proliferating cells) and K14 (tumor cells) and quantification (right) of Ki67⁺ cells/mm² ($n = 4$ Ctrl and 5 CIA1 treated tumors) (**g**). Immunostaining (left) for cleaved caspase 3 (apoptotic cells, arrowheads) and K14 (tumor cells) and quantification (right) of Casp3⁺ cells/mm² ($n = 4$ Ctrl and 5 CIA1-treated tumors) (**h**). Immunostaining of Ctrl and CIA1-treated tumors for K14 (tumor cells) and CD45 (immune cells), Fibronectin 1 (FN1) and CD31 (endothelial cells) (**i**). Quantification of CD45⁺ cells/tumor area ($n = 4$ Ctrl and 6 CIA1-treated tumors) (**j**). Quantification of percentage of CD31⁺ cells/tumor area ($n = 5$ Ctrl and 5 CIA1-treated tumors) (**k**). All images are representative of a minimum of four independent biological replicates each per condition. Scale bar, 50 μm. Data are represented as mean ± s.e.m. P value is calculated using a two-tailed Mann–Whitney U -test.

experimental conditions), *RUNX2* and *ELF3* (Fig. 8g,i). In addition, NR2F2 directly regulated expression of genes regulating key tumor functions, including metabolism (*H6GP*), ECM (*MATN2*) or angiogenesis (*VEGFA*) (Fig. 8g,i).

Discussion

In this study, we identified NR2F2 as an essential regulator of malignant tumor state through promotion of tumor self-renewal, invasion and restriction of tumor differentiation.





In contrast with other TFs regulating skin tumor stemness such as SOX2, TWIST1 and PITX1, which are important for the maintenance of benign and malignant squamous skin tumors, NR2F2 is

only expressed by and controls malignant tumor cells^{13–16}. Whereas NR2F2 knockdown has been shown to decrease cancer cell line proliferation in vitro^{23,30,51,52}, no study has assessed the impact of NR2F2

Fig. 8 | Conservation of NR2F2 function in human SCCs. **a**, Quantification of cell number in A431 Ctrl and NR2F2 shRNA KD1 ($n = 4$ biological replicates). **b**, ALDH activity in A431 Ctrl and NR2F2 shRNA KD1 and KD2 cell lines ($n = 3$ biological replicates). **c**, Wound-healing assay in A431 Ctrl and NR2F2 shRNA KD1 and KD2 cell lines ($n = 3$ biological replicates, 3–4 pictures per well). **d**, mRNA (qPCR) expression of differentiation genes in calcium-switch-induced A431 cells Ctrl and NR2F2 shRNA KD ($n = 4$ for *KRT10* and *IVL*, $n = 3$ for *GRHL1*, *OVOL1*, *HES-1*). **e, f**, Venn diagram of the genes downregulated (**e**) and upregulated (**f**) upon NR2F2 KD in human SCC cell lines (A431 control and NR2F2 shRNA KD1 and KD2 cell lines) and in NR2F2 KO mouse SCC (P values are calculated using two-sided hypergeometric test). **g, h**, mRNA expression (RNA-seq) of downregulated (**g**) and upregulated (**h**) genes following NR2F2 KD in human SCC cell lines. lncRNA, long-noncoding RNA. ChIP-identified NR2F2 direct targets are highlighted with an asterisk ($n = 2$ biological replicates). **i**, A431 NR2F2 ChIP-seq profiles at selected gene loci, including input on top. **j**, TF motifs enriched in ChIP-seq for NR2F2 peaks that were enriched in A431 cells overexpressing NR2F2 compared to input as determined by Homer analysis using known motif search. **k**, Overlap of A431 NR2F2 ChIP-seq peaks with downregulated and upregulated genes in the NR2F2 KD1 human cell line (P values are calculated using two-sided hypergeometric test). Data in **a–d, g, h** are represented as mean \pm s.e.m. (**a–d**). P values are calculated using Mann-Whitney U -test in **c** and two-tailed t -test in other cases.

acute deletion in established tumors in vivo, mimicking the impact that administration of NR2F2 inhibitors might have in a therapeutic setting. Our results revealed that acute inhibition of NR2F2 leads to complete regression of established SCC. These results demonstrate the essential role of NR2F2 in sustaining malignant tumor state maintenance.

The disappearance of SCCs following *Nr2f2* deletion is accompanied by histological signs of tumor differentiation, necrosis and immune infiltration. Our molecular profiling following NR2F2 GOF and loss of function uncovered the gene signature controlled by NR2F2, which regulates essential tumor functions, including EMT, ECM remodeling, immune cell infiltration and tumor differentiation.

NR2F2 regulates expression of several components of the ECM associated with malignant tumor states, such as *Fibronectin 1* (*Fn1*), *Nidogen 1* (*Nid1*), several collagens and lysyl oxidases responsible for collagen fiber crosslinking, which contribute to tumor invasion, EMT and metastasis^{53–56}. Our in vivo study also shows that NR2F2 acts upstream of *Zeb1/2* and *Prrx1*, all key TFs that promote EMT and metastasis^{57–59}.

Tumor regression following acute *Nr2f2* deletion is associated with increased differentiation and expression of K1/K10 in nonproliferative terminally differentiated tumor cells, mirroring the differentiation pattern observed in normal skin and benign papillomas. Notably, our experiments in hSCC cells using a NR2F2 inhibitor or inducible shRNA confirmed that a similar function is conserved in human tumors. In particular, we showed that NR2F2 directly regulates a transcriptional program regulating tumor progression and microenvironment remodeling as well as repressing tumor differentiation. Drug-induced tumor differentiation has been shown to be a very efficient treatment with little side effects for some types of leukemia⁶⁰. Retinoic acid, which induces differentiation of leukemic cells into terminally differentiated granulocytes without much side effects, is now a first-line therapy in combination with arsenic trioxide, leading very frequently to complete remission of this previously incurable disease^{60,61}. While this demonstrated that inducing tumor differentiation could be a safe and very efficient way to treat cancer, very few other examples have been provided in the last decades, in particular in solid tumors. Only recently, thanks to a better understanding of the mechanisms promoting tumor stemness, has the proof of principle that pharmacological induction of tumor differentiation can be used in solid tumors been provided. In a fraction of colorectal cancers presenting *PTPRK–RSPO3* gene fusion, administration of a RSPO3-blocking antibody promotes tumor regression by inducing the differentiation of CSCs into terminally differentiated goblet cells⁶². More recently, it has also been shown that anti-Smoothed inhibitor promotes basal cell carcinoma regression through tumor cell differentiation^{63,64}. Many small-molecule inhibitors and activators targeting nuclear receptors such as NR2F2 are used routinely in clinics in different therapeutic indications, such as anti-estrogen for breast cancer.

The development of NR2F2 inhibitors for anticancer therapy seems to be a very promising strategy, as NR2F2 is expressed in a wide range of aggressive human cancers for which there is an unmet clinical need. Moreover, NR2F2 inhibition in vivo has no apparent side effects on normal adult tissues²⁰ and promotes tumor differentiation, inhibits neoangiogenesis¹⁹, invasion and tumor stemness, all essential hallmarks of cancer functions, demonstrating the promise of targeting NR2F2 in cancer.

Methods

Compliance with ethical regulations. Mouse colonies were maintained in a certified animal facility in accordance with European guidelines. All experiments were approved by the corresponding ethical committee (Commission d'Éthique et du Bien être Animal, Faculty of Medicine, Université Libre de Bruxelles (ULB)), which follows the European Convention for the Protection of Vertebrate Animals used for Experimental and other Scientific Purposes (ETS no.123). The project proposal was submitted to the Ethical Committee for Animal Experimentation for evaluation and approval. The committee consists of internal and external members with expertise regarding ethics, alternative methods to animal experiments, animal health and welfare as well as research techniques, experimental design and statistical analysis. The ULB ERASME Ethical Committee for Animal Experimentation is responsible for evaluating and approving or rejecting all projects involving animal experiments, as an independent body under Belgian legislation (Royal Decree regarding the protection of laboratory animals of 29 May 2013) and European Union Directive 2010/63/EU. For every project proposal, the Ethical Committee for Animal Experimentation takes the so-called 3R principle (replacing, reducing, refining) as its guiding principle and in accordance with European guidelines. Project authorization was approved under no. 665N from the ULB ERASME Ethical Committee for Animal Experimentation. Mice were checked every day and were killed when tumors reached end-point size (1 cm in diameter for all experiments except for 2 cm in diameter for experiments described in Fig. 7e) or if the tumor was ulcerated independently of its size, if the mouse lost >20% of the initial weight or any other sign of distress appeared (based on the general health status and spontaneous activity). None of the experiments performed in this study surpassed the size limit of the tumors. All experiments strictly complied with the protocols approved by the ethical committee.

Mouse strains. *K14Cre*, *K14CreER*, *Lgr5CreER*, *K5CreER*, *KRasLSL-G12D* and *p53^{fl/fl}* mice were imported from the National Cancer Institute mouse repository and The Jackson Laboratory. NOD/SCID, NOD/SCID IL2 and Swiss nude mice were purchased from Charles River. *K14rtta-Nr2f2-IRES-GFP* mice were generated in house. *Nr2f2^{fl/fl}* mice were a generous gift from S. Tsai (Baylor College of Medicine). All mice used in this study were males and females with mixed genetic background. Sex-specific differences were minimized by including similar numbers of male and female animals in all cases.

DMBA/TPA-induced skin tumors. Mice were treated with DMBA and TPA according to standard protocols^{5,10}.

KRas^{LSL-G12D}p53^{fl/fl}-driven skin tumors. Tamoxifen was diluted at 25 mg ml⁻¹ in sunflower seed oil (Sigma). A daily intraperitoneal (i.p.) injection of 2.5 mg of tamoxifen was administered 4 d in a row starting at P28 as previously described to *Lgr5CreER/Kras^{LSL-G12D}/p53^{fl/fl}/Nr2f2^{fl/fl}* mice and two i.p. injections of 2.5 mg of tamoxifen were administered to *K14CreER/Kras^{LSL-G12D}/p53^{fl/fl}/Nr2f2^{fl/fl}* mice. Tumor appearance and size were followed up by daily observation and palpation. Mice were killed when tumor size reached a maximum size of 1 cm, or when mice presented signs of distress.

Collection of human samples. The samples were provided by Erasme Biobank and originate from adult patients who developed head and neck, lung, skin or esophagus SCC or actinic keratosis, as well as corresponding normal skin controls. There was no restriction of age (except that only adult patients were included) or sex and no pre-treated tumors were included. The analyzed samples were collected from surgically removed material, not directly from patients. All samples belong to the Erasme Biobank (B406201525681). The goal of the study was to examine expression and localization of NR2F2 in different contexts. There was no intention of correlation with histopathology tumor grade or tumor aggressiveness. The human collection study was approved by the Erasme Ethical Committee (ref. no. P2015/330/B406201525681).

Immunostaining. Staining was performed on frozen sections or in paraffin-embedded sections according to standardized procedures⁶⁵. Briefly, for immunostaining on frozen sections, tumor tissues were embedded in OCT (Tissue Tek) for cryopreservation. Blocks were sectioned in 4–5- μ m sections using CM3050S cryostat (Leica Microsystems). Fixation was performed using 4% paraformaldehyde. Nonspecific antibody binding was blocked with 5% horse serum, 1% BSA and 0.2% Triton X-100 for 1 h at room temperature. Primary antibodies were incubated overnight at 4°C in blocking buffer. Secondary antibodies were diluted in blocking buffer at 1:400 for 1 h at room temperature. Nuclei were stained with Hoechst (4 mM) and slides were mounted using SafeMount (Labonord). For staining paraffin sections, 4- μ m paraffin sections were deparaffinized and rehydrated. Antigen unmasking was performed in citrate buffer (pH 6) or EDTA buffer (pH 9) at 98°C during 20 min using the PT module. Endogenous peroxidase was blocked using 3% H₂O₂ (Merck) in methanol (VWR) during 20 min at room temperature. Endogenous avidin and biotin were blocked using the Endogenous Blocking kit (Invitrogen) during 20 min at room temperature. Primary antibodies were incubated overnight at 4°C. Anti-rabbit biotinylated secondary antibodies were used, as well as Standard ABC kit and ImmPACT DAB (Vector Laboratories) for the detection of HRP activity. Slides were mounted using SafeMount (Labonord).

The complete list of antibodies used in this study is included in the Reporting Summary.

Image acquisition. Image acquisition was performed on a Zeiss Axio Imager M1 (Thornwood) fluorescence microscope with a Zeiss Axiocam MR3 camera using the Axiovision software release 4.6. Brightness, contrast and picture size were adjusted using Adobe Photoshop CS6 without altering any information.

Quantification of IF and H&E sections. The quantification of K10⁺ tumor cells and laminin-5 gaps in NR2F2 OE papillomas, K8, E-Cad, PHH3, ki67 and BrdU-positive tumor cells was performed on at least four different fields per tumor using ImageJ software (<https://imagej.nih.gov/ij/>).

For quantification of the Zeb1 and Zeb2 content in IHC of tumor sections, we selected at random a minimum of four representative fields from scans of complete cross-sections of the tumor, used NDP.view2 software to visualize them (<https://www.hamamatsu.com/eu/en/product/type/U12388-01/index.html>) and counted the number of Zeb1⁺ and Zeb2⁺ epithelial tumor cells versus all epithelial cells.

The quantification of K10⁺ tumor areas in NR2F2 KO tumors and respective controls and of the percentage of keratin content in Figs. 5 and 7 was performed using mosaic images of a whole tumor section. In all cases, areas were quantified using ImageJ software. For quantification of keratin content in tumor sections, we used scans of complete cross-sections of the tumor and NDP.view2 software.

Histopathological analysis on NR2F2 KO tumors. In Fig. 4h, the mitotic index was quantified on ten fields at $\times 400$ and divided by ten to obtain the value per high-power field, which was used to calculate the mean of the Ctrl and NR2F2 KO groups. The results of the other parameters (spongiosis, necrosis and keratinization) are based on a semi-quantitative analysis that took into account the stratification of samples into negative (presence of the morphological feature in <20% of the tumor area) or positive (presence of the morphological feature in >20% of the tumor area). To calculate *P* values, we used the Mann–Whitney *U*-test for the mitotic index and Fisher's exact test in all other cases.

Tumor digestion and FACS staining. Tumors were dissected mechanically, digested with collagenase and stained for cell surface markers according to standard protocols⁶⁶. Cell sorting was performed with a FACS Aria cell sorter (BD Biosciences). The complete list of antibodies used in this study is included in the Reporting Summary.

Annexin V staining. We used the FITC annexin V Apoptosis Detection kit I (BD Pharmingen, cat. no. 556547). Briefly, after tumor digestion, cells were stained with Epcam/CD326 APC/Cy7 (BioLegend, 118218 Clone G8.8) to identify Tumor Epithelial Cells. Subsequently, cells were counted using a Neubauer cell counting chamber. As recommended by the manufacturer, 100,000 cells were used for FITC annexin V/PI staining according to the standard protocol.

Western blot. SDS-PAGE and western blot were performed according to standard protocols. Five percent milk was used as a blocking agent. The complete list of

antibodies used in this study is included in the Reporting Summary. Western Lightning Plus ECL (PerkinElmer) was used as a substrate.

Cell culture. SK-MES-1 (human lung SCC) and A431 (human skin SCC) cells were maintained in EMEM supplemented with 2 mM glutamine and 10% FBS. Kyse-70 (human esophagus SCC) cells were maintained in RPMI 1640 supplemented with 2 mM glutamine and 10% FBS. The 293T cells were maintained in DMEM (Gibco) supplemented with 10% FBS, 2 mM glutamine, 100 U ml⁻¹ Pen/Strep solution, MEM Non-Essential Amino Acids Solution and pyruvate. All cell lines were acquired from the DSMZ-German Collection of Microorganisms and Cell Cultures.

Generation of NR2F2 OE lines and inducible shRNA lines. The NR2F2 rescue experiments described in Fig. 3 and Extended Data Fig. 3 were performed by cloning the coding sequence of NR2F2 fused to a C-terminal 3HA tag in the pLX302-EF1a vector (constitutive expression). The ChIP experiments described in Fig. 8 and Extended Data Fig. 7 were performed by cloning the coding sequence of NR2F2 fused to an N-terminal 3HA tag in the pLVX-TetOne-Puro Vector (doxycycline inducible; Clontech, cat. no. 631849). The shRNA experiments described in Fig. 8 and Extended Data Fig. 7 were performed using the SMARTvector Inducible Human NR2F2 PGK-TurboGFP shRNA construct (doxycycline inducible; Horizon Discovery Biosciences, cat. no. V3SH11252-225716276; sequence included in Extended Data Table 1). For the generation of cell lines with stable integration of the constructs, VSVg pseudotyped lentivirus was produced by Lipofectamine 2000 transfection (Invitrogen) of HEK293T cells with the vector encoding for full-length NR2F2 or the inducible NR2F2 shRNA vector and the helper plasmids pMD2-VSVg and pPAX2 (Addgene plasmid 12259 and 12260, respectively). At 48 h after transfection, we collected the viral supernatant and infected the target cell lines using standard methods. After 1 week of puromycin selection, cells were tested for NR2F2 expression by western blot. For the inducible constructs, 1 μ M doxycycline was used.

Generation of NR2F2 CRISPR/CAS9 knockout in hSCC cells. We generated the NR2F2 KO cell lines by designing four guide RNAs targeting exon 2. The most efficient gRNAs were predicted using the MIT CRISPR design tool (Zhang Laboratory, MIT 2015, now discontinued). The gRNA sequences were cloned as double-stranded oligonucleotides in the pSpCas9n (BB)-2A-GFP (PX461) plasmid (Addgene plasmid 48140), expressing the Cas9 D10A mutant and EGFP simultaneously. We designed the guides to generate a deletion of about 400 bp. The sequence of the single-guide RNAs is provided in Extended Data Table 1. We used transient transfection and FACS to establish single-cell clones. As soon as single-cell clones were visible, we amplified them, extracted genomic DNA and probed them by PCR with a combination of primers detecting the presence or absence of the deletion. We further validated the deleted clones by sequencing the deletion site using PCR primers flanking the position of the gRNAs, ensuring that the occurring deletion generated a frame shift in the coding sequence. We also validated the NR2F2 KO clones by western blot.

Tumor transplantation assays. Tumor cells were collected in 4°C medium after FACS or counted after tumor digestion and collected in PBS plus 2% FBS. For the calculation of TPC, cells at known dilutions were resuspended in Matrigel (E1270, 970 mg ml⁻¹; Sigma) and injected subcutaneously into NOD/SCID mice. Secondary tumors were detected by palpation every week and their size was monitored until tumor reached 1 cm or when mice presented signs of distress. The mice were subsequently killed and the number of secondary tumors was quantified.

Calcium-switch assay. To promote cell differentiation of confluent A431 cells, cells were first incubated overnight in low-calcium medium containing 10% calcium-free FBS. Next, the calcium medium level was raised to the final concentration of Ca²⁺ of 1.5 mM for 48 h⁶⁶.

ALDH activity. To evaluate ALDH activity, cells cultured in ultra-low adherent plates (*n* = 500,000 cells per test) were collected and processed according to the manufacturer's instruction (Aldered 588-A, SCR150, Merck).

Wound-healing assay. Wound-healing assays were performed to evaluate the impact of NR2F2 knockdown on the migration of A431 NR2F2 shRNA 1 and 2 SCC cell lines. The assay was performed in 24-well plates (*n* = 3 wells per condition)⁶⁷. At confluency, cells were serum starved (1% FBS medium) for 24 h before manually creating a wound with a 200- μ l tip. Next, cells were washed twice with PBS and re-incubated in 1% FBS medium. To evaluate wound closure, pictures were processed using ImageJ software.

CIA1 treatment. CIA1 was obtained from MolPort (molport-002-661-412). All treatments were performed as previously described⁶⁴. For cell viability assay, cells were seeded in a 96-well plate with transparent bottom at 3,000 cells per well, adding the inhibitor the following day. After 72 h of incubation, cell viability was assessed using CellTiter-Glo Luminescent Cell Viability Assay (G7570, Promega) according to manufacturer's instructions.

For the in vivo TPC assay, A431 cells were pre-treated with 4 μM CIA1 for 12 h before the graft. After grafting, mice were treated for 2 weeks daily with 2.6 mg kg^{-1} CIA1 dissolved in 10% (2-hydroxypropyl)- β -cyclodextrin (332593, Sigma-Aldrich) in sterile saline solution and administered by i.p. injection. The end point of the experiment was at 10 weeks after grafting, unless tumor size reached the limit point before. For the experiments of CIA1 treatment in established tumors, we grafted 10^5 A431 cells into immunodeficient mice. Once tumor size reached a palpable size (diameter of about 0.2–0.3 cm), we started daily treatment with CIA1 as previously described. Tumor size was measured weekly with a caliper during the entire experimental process. Tumor volume was calculated with the formula: $V = \pi \times (d^2 \times D) / 6$, where d is the minor tumor axis and D is the major tumor axis. At the end of the experiment, mice were killed and tumor tissue was removed for further examination. DMSO injection was used as control condition.

Metastasis assay. The different FACS-isolated tumor cell subpopulations or cultured cell lines were collected in 4°C medium. Cells were resuspended in PBS in 50 μl PBS and injected into the tail vein of *NOD/SCID/IL2R γ* null mice (50,000 cells per injection for mouse primary SCC cells; 100,000 cells for SK-MES-1 and corresponding KO and rescue lines). Mice were killed at 30 d (for mouse SCC cells; Fig. 6j) and 60 d (for lung hSCC cells; Fig. 6k) and lungs were analyzed to detect the presence of metastases. The number of metastases was quantified on ten cryosections per lung (separated by 100 μm) and presented as number of metastases per lung. The metastases were characterized by K14 and vimentin expression (mouse SCC cells) or pancytokeratin and Ku80 expression (hSCC cells) by immunofluorescence.

RNA extraction and real-time PCR. RNA extraction from FACS-isolated cells was performed using RNeasy micro kit (QIAGEN) according to the manufacturer's recommendations. qRT-PCR analysis was performed under standard conditions. All primer sequences are provided in Extended Data Table 1.

Microarray analysis. Total RNA was analyzed using the Mouse Genome 430 PM strip arrays from Affymetrix at the Functional Genomics Core of IRB Barcelona microarray facility (transcriptional profiling of NR2F2 OE papillomas and NR2F2 KO carcinomas) or at the VIB MicroArray Facility in Leuven (transcriptional profiling of CD34⁺ cells from SCC and papilloma). To normalize the data, the robust multi-array average expression method from the affy package was used⁶⁸. Two different biological replicates from Ctrl SCC and NR2F2 KO SCC tumor epithelial cells and for Pap Ctrl and Pap GOF were analyzed. Genes with a fold change in linear scale of expression ≥ 2 were considered as upregulated/downregulated. The analysis yielded a total of 1,029 downregulated genes and 991 upregulated genes in loss of function SCCs; 632 upregulated and 1,559 downregulated genes in the papilloma GOF models, respectively. For the CD34⁺ array, we analyzed four different biological replicates for SCC and three for papillomas. Genes with a fold change in linear scale of expression ≥ 2 were considered as regulated. The analysis yielded a total of 184 upregulated genes and 143 downregulated genes in CD34⁺ cells from SCC compared to papilloma.

RNA-sequencing. RNA extraction from FACS-isolated cells was performed using RNeasy micro kit (QIAGEN) according to the manufacturer's recommendations. Before sequencing, the quality of RNA was evaluated by Bioanalyzer 2100 (Agilent). Indexed complementary DNA libraries were obtained using the Ovation Solo RNA-seq Systems (NuGen) following manufacturer's recommendations.

The multiplexed libraries were loaded on flow cells and sequences were produced using a NovaSeq 6000 S2 Reagent kit (200 cycles from a NovaSeq 6000 System, Illumina). Approximately 19 million paired-end reads per sample were generated and quality checks were performed with FastQC (<https://www.bioinformatics.babraham.ac.uk/projects/fastqc/>). The adaptor sequences and low-quality regions were trimmed by Trimmomatic⁶⁹. Trimmed reads were mapped against the mouse reference genome (GRCh38/hg38) using STAR software⁷⁰ to generate read alignments for each sample. Annotations for GRCh38.87 were obtained from <ftp://ensembl.org>. After transcript assembling, gene-level counts were obtained using HTseq (v.0.11.1)⁷¹ and normalized to 20 million of aligned reads. Average expression for each gene for the different tumor cell populations was computed based on at least two biological replicates and fold changes were calculated between the subpopulations. For the experiments described in Fig. 8, genes with a fold change of expression ≥ 1.5 were considered as upregulated and those having a fold change of expression ≤ 0.66 were considered downregulated.

ChIP-sequencing. For ChIP-seq, cells were collected after induction of doxycycline (1 $\mu\text{g ml}^{-1}$). Cells were fixed with fresh 200 mM solution of Di(*N*-succinimidyl) glutarate for 20 min and 37% formaldehyde for 8 min. Fixed cells were quenched with 100 μl of Glycine Stop solution (10X) (Active Motif) for 5 min. Chromatin shearing was performed using the ChIP-IT Express kit (Active Motif) according to the manufacturer's recommendations. ChIP was performed using Dynabeads Protein G (Invitrogen) and HA-tag antibody (Abcam, ab9110). Purification was performed using the iPure kit v2 (Diagenode). The sequencing library was constructed using NEB Next Ultra II DNA library Prep kit for Illumina (Biolabs)

according to manufacturer's instructions and subsequently sequenced on a Novaseq 6000 platform (Illumina).

ChIP-sequencing analysis. Before starting the alignment and downstream analysis, quality checking was performed by FastQC (<https://www.bioinformatics.babraham.ac.uk/projects/fastqc/>). The alignment and peak calling were managed by Consortium des Équipements de Calcul Intensif. Adaptor sequences and low-quality regions were removed with Trimmomatic⁶⁹ (v.1.11) paired-end mode using options 'HEADCROP:10 CROP:65 ILLUMINACLIP:adaptor.file:2:30:10 LEADING:3 TRAILING:3 SLIDINGWINDOW:4:15 MINLEN:50'. Trimmed reads were then aligned to human reference genome hg38 using Bowtie2 (ref. ⁷²) (v.2.3.4.2) using options '-X 2000 -q -p 6 -t -fr -very-sensitive -no-discordant -no-unal -no-mixed'. Mitochondrial reads, reads from unmapped and random contigs, reads without unique alignment, reads with a mapping quality <20 and reads which were not properly mapped were removed using SAMtools⁷³ (v.1.11). Duplicate reads were removed by Picard Mark Duplicates (<http://broadinstitute.github.io/picard/>). Peak calling was performed by macs2 (ref. ⁷⁴) (v.2.2.5) using options '-f BAMPE -g hs -p 0.01 -nomodel'. Blacklisted regions were filtered out by BEDtools⁷⁵ intersect (v.2.27.1).

The raw count was globally normalized into count per 1 million. Peaks were associated with genes with GREAT⁷⁶ software (v.4.0.4) with the following parameters: 5.0 kb in proximal upstream, 1.0 kb in proximal downstream and up to 100.0 kb in distal.

De novo motif prediction was performed using findMotifsGenome.pl program in HOMER⁷⁷ (v.4.10) software using parameters '-size -250,250 -S 15 -len 6,8,10,12'.

Gene Ontology analysis. Gene Ontology analysis based on the datasets from the transcriptional profiling of mouse SCC was performed using the Enrichr online software (<https://maayanlab.cloud/Enrichr/>)^{78,79}.

TCGA data acquisition and analysis. The Cervical SCC dataset, disclosed by The Cancer Genome Atlas (TCGA), was downloaded from the National Cancer Institute portal at <https://portal.gdc.cancer.gov>. It contains RNA-seq raw count data as well as clinical information. Raw count expression data were normalized by computing the log₂ transcripts per million method.

For statistical analysis, gene expression data were stratified into two groups on the basis of NR2F2 expression. The top-tertile cutoff point was defined as the third tertile value of NR2F2 distribution. Samples with an expression level higher or lower than the selected cutoff-point threshold were classified as 'high' and 'low', respectively. Statistical significance of the difference in survival was computed using the Cox proportional hazard model and the log-rank test *P* value reported on Kaplan–Meier survival curves⁸⁰.

All analyses were performed on the R platform (v.3.4.4). All statistical analyses were performed as two-sided.

For the survival analysis in correlation with NR2F2 signature, the Cervical SCC TCGA dataset with at least 100 patients was downloaded from the National Cancer Institute portal at <https://portal.gdc.cancer.gov>. Raw count expression data were normalized by computing the log₂ transcripts per million method. Only primary tumors were kept for the analysis (metastatic samples were removed from the analysis).

Statistics and reproducibility. The sample size was chosen based on previous experience in the laboratory for each experiment to yield high power to detect specific effects. No statistical methods were used to predetermine sample size. No data were excluded from analyses. We did not test for normality of datasets. For in vivo studies on primary mouse models, animals were chosen based on correct genotypes. All animals started the treatment with DMBA/TPA at 6–8 weeks of age or were induced with tamoxifen at 28–35 d after birth. Sex-specific differences were minimized by including similar numbers of male and female animals in all cases. Investigators were blinded to mouse genotypes during the analysis, imaging and quantifications (histology analysis, quantifications and FACS).

Two-tailed Mann–Whitney *U*-test, Welch's *t*-test, one-tailed *t*-test, unpaired *t*-test, Fisher's exact test, mixed-model two-way ANOVA and tumor-onset analysis (Kaplan–Meier) were performed using GraphPad Prism v.8 for Mac (GraphPad Software, www.graphpad.com). The corresponding tests used are annotated in figure legends. The TPC frequency was computed using ELDA online software as previously described⁸¹, reporting the stem cells estimate number (TPC) and the *P* value of the chi-squared test (<http://bioinf.wehi.edu.au/software/elda/>). All statistical analyses are based on biological replicates (corresponding to *n* indicated in the text, figures or figure legends). No technical replicates were used for statistical tests. All immunostaining experiments reported in the manuscript are representative of at least four independent experiments (four control and four KO/NR2F2 OE samples). Microarray, RNA-seq and ChIP-seq experiments were performed in duplicate. All western blot images represent results obtained in at least three replicates, unless otherwise specified. The images in Extended Data Fig. 7b–d are representative of three independent experiments. Unprocessed western blot images are included in source data.

Reporting Summary. Further information on research design is available in the Nature Research Reporting Summary linked to this article.

Data availability

All the raw microarray and sequencing data have been deposited in the Gene Expression Omnibus under the following accession codes: GSE164605 (reference series of the whole data), GSE175726 (human RNA-seq), GSE164597 (microarray carcinoma and papilloma CSCs), GSE164602 (microarray papilloma GOF versus Ctrl and carcinoma loss of function versus Ctrl), GSE175724 (ChIP-seq). All other relevant data are available from the corresponding author upon reasonable request. Source data are provided with this paper.

Received: 3 January 2021; Accepted: 8 October 2021;
Published online: 22 November 2021

References

- Alam, M. & Ratner, D. Cutaneous squamous-cell carcinoma. *N. Engl. J. Med.* **344**, 975–983 (2001).
- Sanchez-Danes, A. & Blanpain, C. Deciphering the cells of origin of squamous cell carcinomas. *Nat. Rev. Cancer* **18**, 549–561 (2018).
- Owens, D. M. & Watt, F. M. Contribution of stem cells and differentiated cells to epidermal tumors. *Nat. Rev. Cancer* **3**, 444–451 (2003).
- Perez-Losada, J. & Balmain, A. Stem-cell hierarchy in skin cancer. *Nat. Rev. Cancer* **3**, 434–443 (2003).
- Abel, E. L., Angel, J. M., Kiguchi, K. & DiGiovanni, J. Multi-stage chemical carcinogenesis in mouse skin: fundamentals and applications. *Nat. Protoc.* **4**, 1350–1362 (2009).
- Kemp, C. J. Multistep skin cancer in mice as a model to study the evolution of cancer cells. *Semin. Cancer Biol.* **15**, 460–473 (2005).
- Valent, P. et al. Cancer stem cell definitions and terminology: the devil is in the details. *Nat. Rev. Cancer* **12**, 767–775 (2012).
- Beck, B. & Blanpain, C. Unravelling cancer stem cell potential. *Nat. Rev. Cancer* **13**, 727–738 (2013).
- Beck, B. et al. A vascular niche and a VEGF-Nrp1 loop regulate the initiation and stemness of skin tumors. *Nature* **478**, 399–403 (2011).
- Lapouge, G. et al. Skin squamous cell carcinoma propagating cells increase with tumor progression and invasiveness. *EMBO J.* **31**, 4563–4575 (2012).
- Malanchi, I. et al. Cutaneous cancer stem cell maintenance is dependent on β -catenin signalling. *Nature* **452**, 650–653 (2008).
- Schober, M. & Fuchs, E. Tumor-initiating stem cells of squamous cell carcinomas and their control by TGF- β and integrin/focal adhesion kinase (FAK) signaling. *Proc. Natl Acad. Sci. USA* **108**, 10544–10549 (2011).
- Beck, B. et al. Different levels of Twist1 regulate skin tumor initiation, stemness, and progression. *Cell Stem Cell* **16**, 67–79 (2015).
- Boumahdi, S. et al. SOX2 controls tumor initiation and cancer stem-cell functions in squamous-cell carcinoma. *Nature* **511**, 246–250 (2014).
- Sastre-Perona, A. et al. De novo PITX1 expression controls bi-stable transcriptional circuits to govern self-renewal and differentiation in squamous cell carcinoma. *Cell Stem Cell* **24**, 390–404 (2019).
- Siegle, J. M. et al. SOX2 is a cancer-specific regulator of tumor initiating potential in cutaneous squamous cell carcinoma. *Nat. Commun.* **5**, 4511 (2014).
- Lin, F. J., Qin, J., Tang, K., Tsai, S. Y. & Tsai, M. J. Coup d'Etat: an orphan takes control. *Endocr. Rev.* **32**, 404–421 (2011).
- Pereira, F. A., Tsai, M. J. & Tsai, S. Y. COUP-TF orphan nuclear receptors in development and differentiation. *Cell Mol. Life Sci.* **57**, 1388–1398 (2000).
- Qin, J., Chen, X., Xie, X., Tsai, M. J. & Tsai, S. Y. COUP-TFII regulates tumor growth and metastasis by modulating tumor angiogenesis. *Proc. Natl Acad. Sci. USA* **107**, 3687–3692 (2010).
- Qin, J., Chen, X., Yu-Lee, L. Y., Tsai, M. J. & Tsai, S. Y. Nuclear receptor COUP-TFII controls pancreatic islet tumor angiogenesis by regulating vascular endothelial growth factor/vascular endothelial growth factor receptor-2 signaling. *Cancer Res.* **70**, 8812–8821 (2010).
- Xie, X., Tang, K., Yu, C. T., Tsai, S. Y. & Tsai, M. J. Regulatory potential of COUP-TFs in development: stem/progenitor cells. *Semin. Cell Dev. Biol.* **24**, 687–693 (2013).
- Hawkins, S. M. et al. Expression and functional pathway analysis of nuclear receptor NR2F2 in ovarian cancer. *J. Clin. Endocrinol. Metab.* **98**, E1152–E1162 (2013).
- Polvani, S. et al. COUP-TFII in pancreatic adenocarcinoma: clinical implication for patient survival and tumor progression. *Int. J. Cancer* **134**, 1648–1658 (2014).
- Qin, J., Tsai, S. & Tsai, M. J. COUP-TFII, a prognostic marker and therapeutic target for prostate cancer. *Asian J. Androl.* **15**, 360–361 (2013).
- Ding, W. et al. Overexpression of COUP-TFII suppresses proliferation and metastasis of human gastric cancer cells. *Mol. Med. Rep.* **17**, 2393–2401 (2018).
- Litchfield, L. M., Appana, S. N., Datta, S. & Klinge, C. M. COUP-TFII inhibits NF- κ B activation in endocrine-resistant breast cancer cells. *Mol. Cell Endocrinol.* **382**, 358–367 (2014).
- Shin, S. W. et al. Clinical significance of chicken ovalbumin upstream promoter-transcription factor II expression in human colorectal cancer. *Oncol. Rep.* **21**, 101–106 (2009).
- Wang, C. et al. High expression of COUP-TF II cooperated with negative Smad4 expression predicts poor prognosis in patients with colorectal cancer. *Int. J. Clin. Exp. Pathol.* **8**, 7112–7121 (2015).
- Zhang, C., Han, Y., Huang, H., Qu, L. & Shou, C. High NR2F2 transcript level is associated with increased survival and its expression inhibits TGF- β -dependent epithelial–mesenchymal transition in breast cancer. *Breast Cancer Res. Treat.* **147**, 265–281 (2014).
- Qin, J. et al. COUP-TFII inhibits TGF- β -induced growth barrier to promote prostate tumorigenesis. *Nature* **493**, 236–240 (2013).
- Latil, M. et al. Cell-type-specific chromatin states differentially prime squamous cell carcinoma tumor-initiating cells for epithelial to mesenchymal transition. *Cell Stem Cell* **20**, 191–204 (2017).
- Nassar, D., Latil, M., Boeckx, B., Lambrechts, D. & Blanpain, C. Genomic landscape of carcinogen-induced and genetically induced mouse skin squamous cell carcinoma. *Nat. Med.* **21**, 946–954 (2015).
- Lapouge, G. et al. Identifying the cellular origin of squamous skin tumors. *Proc. Natl Acad. Sci. USA* **108**, 7431–7436 (2011).
- White, A. C. et al. Defining the origins of Ras/p53-mediated squamous cell carcinoma. *Proc. Natl Acad. Sci. USA* **108**, 7425–7430 (2011).
- Caulin, C., Bauluz, C., Gandarillas, A., Cano, A. & Quintanilla, M. Changes in keratin expression during malignant progression of transformed mouse epidermal keratinocytes. *Exp. Cell Res.* **204**, 11–21 (1993).
- Marcato, P., Dean, C. A., Giacomantonio, C. A. & Lee, P. W. Aldehyde dehydrogenase: its role as a cancer stem cell marker comes down to the specific isoform. *Cell Cycle* **10**, 1378–1384 (2011).
- Marcato, P. et al. Aldehyde dehydrogenase activity of breast cancer stem cells is primarily due to isoform ALDH1A3 and its expression is predictive of metastasis. *Stem Cells* **29**, 32–45 (2011).
- Pastushenko, I. et al. Identification of the tumor transition states occurring during EMT. *Nature* **556**, 463–468 (2018).
- Vaillant, F. et al. The mammary progenitor marker CD61/ β 3 integrin identifies cancer stem cells in mouse models of mammary tumorigenesis. *Cancer Res.* **68**, 7711–7717 (2008).
- van Kempen, L. C. et al. Activated leukocyte cell adhesion molecule/CD166, a marker of tumor progression in primary malignant melanoma of the skin. *Am. J. Pathol.* **156**, 769–774 (2000).
- Xiao, M. et al. Cancer stem-like cell related protein CD166 degrades through E3 ubiquitin ligase ChIP in head and neck cancer. *Exp. Cell Res.* **353**, 46–53 (2017).
- Gujral, T. S. et al. A noncanonical Frizzled2 pathway regulates epithelial–mesenchymal transition and metastasis. *Cell* **159**, 844–856 (2014).
- Moll, R., Franke, W. W., Schiller, D. L., Geiger, B. & Krepler, R. The catalog of human cytokeratins: patterns of expression in normal epithelia, tumors and cultured cells. *Cell* **31**, 11–24 (1982).
- Wang, L. et al. Small-molecule inhibitor targeting orphan nuclear receptor COUP-TFII for prostate cancer treatment. *Sci. Adv.* **6**, eaaz8031 (2020).
- Ma, I. & Allan, A. L. The role of human aldehyde dehydrogenase in normal and cancer stem cells. *Stem Cell Rev. Rep.* **7**, 292–306 (2011).
- Minn, I. et al. A red-shifted fluorescent substrate for aldehyde dehydrogenase. *Nat. Commun.* **5**, 3662 (2014).
- Pillai, S., Bikle, D. D., Mancianti, M. L., Cline, P. & Hincenbergs, M. Calcium regulation of growth and differentiation of normal human keratinocytes: modulation of differentiation competence by stages of growth and extracellular calcium. *J. Cell Physiol.* **143**, 294–302 (1990).
- Hennings, H. et al. Calcium regulation of growth and differentiation of mouse epidermal cells in culture. *Cell* **19**, 245–254 (1980).
- Angel, P., Szabowski, A. & Schorpp-Kistner, M. Function and regulation of AP-1 subunits in skin physiology and pathology. *Oncogene* **20**, 2413–2423 (2001).
- Ito, Y., Bae, S. C. & Chuang, L. S. The RUNX family: developmental regulators in cancer. *Nat. Rev. Cancer* **15**, 81–95 (2015).
- Qin, J., Tsai, S. Y. & Tsai, M. J. The critical roles of COUP-TFII in tumor progression and metastasis. *Cell Biosci.* **4**, 58 (2014).
- Zheng, J. et al. Knockdown of COUP-TFII inhibits cell proliferation and induces apoptosis through upregulating BRCA1 in renal cell carcinoma cells. *Int. J. Cancer* **139**, 1574–1585 (2016).
- Alečković, M. et al. Identification of Nidogen 1 as a lung metastasis protein through secretome analysis. *Genes Dev.* **31**, 1439–1455 (2017).
- Barker, H. E., Cox, T. R. & Erler, J. T. The rationale for targeting the LOX family in cancer. *Nat. Rev. Cancer* **12**, 540–552 (2012).
- Knowles, L. M. et al. Integrin α v β 3 and fibronectin upregulate Slug in cancer cells to promote clot invasion and metastasis. *Cancer Res.* **73**, 6175–6184 (2013).
- Levental, K. R. et al. Matrix crosslinking forces tumor progression by enhancing integrin signaling. *Cell* **139**, 891–906 (2009).
- Krebs, A. M. et al. The EMT-activator Zeb1 is a key factor for cell plasticity and promotes metastasis in pancreatic cancer. *Nat. Cell Biol.* **19**, 518–529 (2017).

58. Ocana, O. H. et al. Metastatic colonization requires the repression of the epithelial–mesenchymal transition inducer Prrx1. *Cancer Cell* **22**, 709–724 (2012).
59. Stemmler, M. P., Eccles, R. L., Brabletz, S. & Brabletz, T. Non-redundant functions of EMT transcription factors. *Nat. Cell Biol.* **21**, 102–112 (2019).
60. de The, H. Differentiation therapy revisited. *Nat. Rev. Cancer* **18**, 117–127 (2018).
61. Degos, L. et al. All-trans-retinoic acid as a differentiating agent in the treatment of acute promyelocytic leukemia. *Blood* **85**, 2643–2653 (1995).
62. Storm, E. E. et al. Targeting PTPRK-RSPO3 colon tumors promotes differentiation and loss of stem-cell function. *Nature* **529**, 97–100 (2016).
63. Biehls, B. et al. A cell identity switch allows residual BCC to survive Hedgehog pathway inhibition. *Nature* **562**, 429–433 (2018).
64. Sanchez-Danes, A. et al. A slow-cycling LGR5 tumor population mediates basal cell carcinoma relapse after therapy. *Nature* **562**, 434–438 (2018).
65. Pastushenko, I. et al. Fat1 deletion promotes hybrid EMT state, tumor stemness and metastasis. *Nature* **589**, 448–455 (2021).
66. Sallee, J. L. & Burridge, K. Density-enhanced phosphatase 1 regulates phosphorylation of tight junction proteins and enhances barrier function of epithelial cells. *J. Biol. Chem.* **284**, 14997–15006 (2009).
67. Wu, B. et al. Baicalein mediates inhibition of migration and invasiveness of skin carcinoma through Ezrin in A431 cells. *BMC Cancer* **11**, 527 (2011).
68. Gautier, L., Cope, L., Bolstad, B. M. & Irizarry, R. A. affy: analysis of Affymetrix GeneChip data at the probe level. *Bioinformatics* **20**, 307–315 (2004).
69. Bolger, A. M., Lohse, M. & Usadel, B. Trimmomatic: a flexible trimmer for Illumina sequence data. *Bioinformatics* **30**, 2114–2120 (2014).
70. Dobin, A. et al. STAR: ultrafast universal RNA-seq aligner. *Bioinformatics* **29**, 15–21 (2013).
71. Anders, S., Pyl, P. T. & Huber, W. HTSeq: a Python framework to work with high-throughput sequencing data. *Bioinformatics* **31**, 166–169 (2015).
72. Langmead, B. & Salzberg, S. L. Fast gapped-read alignment with Bowtie 2. *Nat. Methods* **9**, 357–359 (2012).
73. Li, H. et al. The sequence alignment/map format and SAMtools. *Bioinformatics* **25**, 2078–2079 (2009).
74. Zhang, Y. et al. Model-based analysis of ChIP-seq (MACS). *Genome Biol.* **9**, R137 (2008).
75. Quinlan, A. R. & Hall, I. M. BEDTools: a flexible suite of utilities for comparing genomic features. *Bioinformatics* **26**, 841–842 (2010).
76. McLean, C. Y. et al. GREAT improves functional interpretation of cis-regulatory regions. *Nat. Biotechnol.* **28**, 495–501 (2010).
77. Heinz, S. et al. Simple combinations of lineage-determining transcription factors prime cis-regulatory elements required for macrophage and B cell identities. *Mol. Cell* **38**, 576–589 (2010).
78. Chen, E. Y. et al. Enrichr: interactive and collaborative HTML5 gene list enrichment analysis tool. *BMC Bioinformatics* **14**, 128 (2013).
79. Kuleshov, M. V. et al. Enrichr: a comprehensive gene set enrichment analysis web server 2016 update. *Nucleic Acids Res.* **44**, W90–W97 (2016).
80. Gendoo, D. M. et al. Genefu: an R/Bioconductor package for computation of gene expression-based signatures in breast cancer. *Bioinformatics* **32**, 1097–1099 (2016).
81. Hu, Y. & Smyth, G. K. ELDA: extreme limiting dilution analysis for comparing depleted and enriched populations in stem cell and other assays. *J. Immunol. Methods* **347**, 70–78 (2009).

Acknowledgements

We are grateful to the Erasme Hospital Biobank (Brussels, Belgium; BE_BERA1; Biobanque Hôpital Erasme-ULB; BE_NBW1; Biothèque Wallonie Bruxelles); BBMRI–ERIC for providing a large number of human tumor samples. We thank S.Y. Tsai (Department of Molecular and Cellular Biology, Baylor College of Medicine) for kindly sharing the NR2F2^{fl/fl} mice. We thank Blanpain laboratory members for their constructive comments on the manuscript. We thank the animal house facility from the ULB (Erasmus campus). C.B. is an investigator of WELBIO. F.M. was supported by a National Fund for Scientific Research (FNRS) postdoctoral fellowship and by TELEVIE. G.L. was supported by an FNRS postdoctoral fellowship and by TELEVIE. This work was supported by WELBIO, the FNRS, TELEVIE, the PAI program (P7/03-CanEpi), the ERC Advanced Grant (agreement ID 885093), the ULB Fondation and the Fondation Baillet Latour. The Center for Microscopy and Molecular Imaging is supported by the Fonds Yvonne Boël, by the European Regional Development Fund and the Walloon Region (Wallonia-biomed; grant no. 411132-957270; 'CMMI-ULB').

Author contributions

C.B., F.M., G.L. and C.S. designed the experiments and performed data analysis. F.M., C.S. and G.L. performed most of the experiments. B.D. started the project. B.D., S.G., I.P., J.B., M.M., A.B., Y.S. and M.Raphaël contributed to the experiments. S.R., J.A. and I.S. provided hSCC samples and performed histological analysis. Y.B. and C.S. performed TCGA data acquisition and analysis. E.N., M. Rozzi, B.D., V.M. and F.R. provided technical support. C.D. provided technical support for cell sorting. G.L. and J.V. contributed to discussion and to preparation of the manuscript. C.B. and F.M. wrote the manuscript.

Competing interests

C.B. is founder and advisor of ChromaCure SA, which develops drugs targeting NR2F2. J.V. and M.M. are employees of ChromaCure. C.B. owns shares in ChromaCure. The remaining authors declare no competing interests.

Additional information

Extended data is available for this paper at <https://doi.org/10.1038/s43018-021-00287-5>.

Supplementary information The online version contains supplementary material available at <https://doi.org/10.1038/s43018-021-00287-5>.

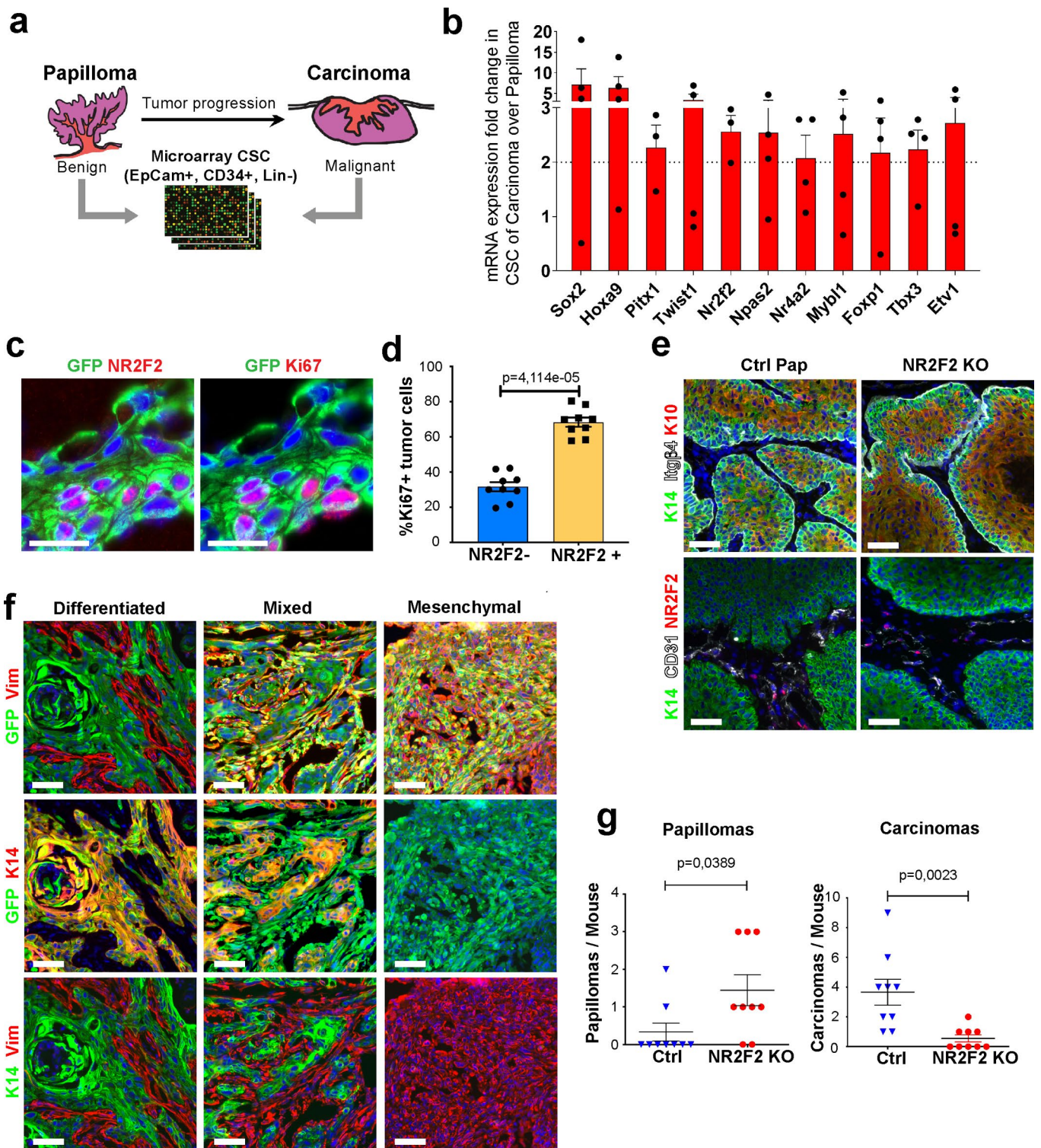
Correspondence and requests for materials should be addressed to Cédric Blanpain.

Peer review information *Nature Cancer* thanks Salvador Benitah, Nick Barker and the other, anonymous, reviewer(s) for their contribution to the peer review of this work.

Reprints and permissions information is available at www.nature.com/reprints.

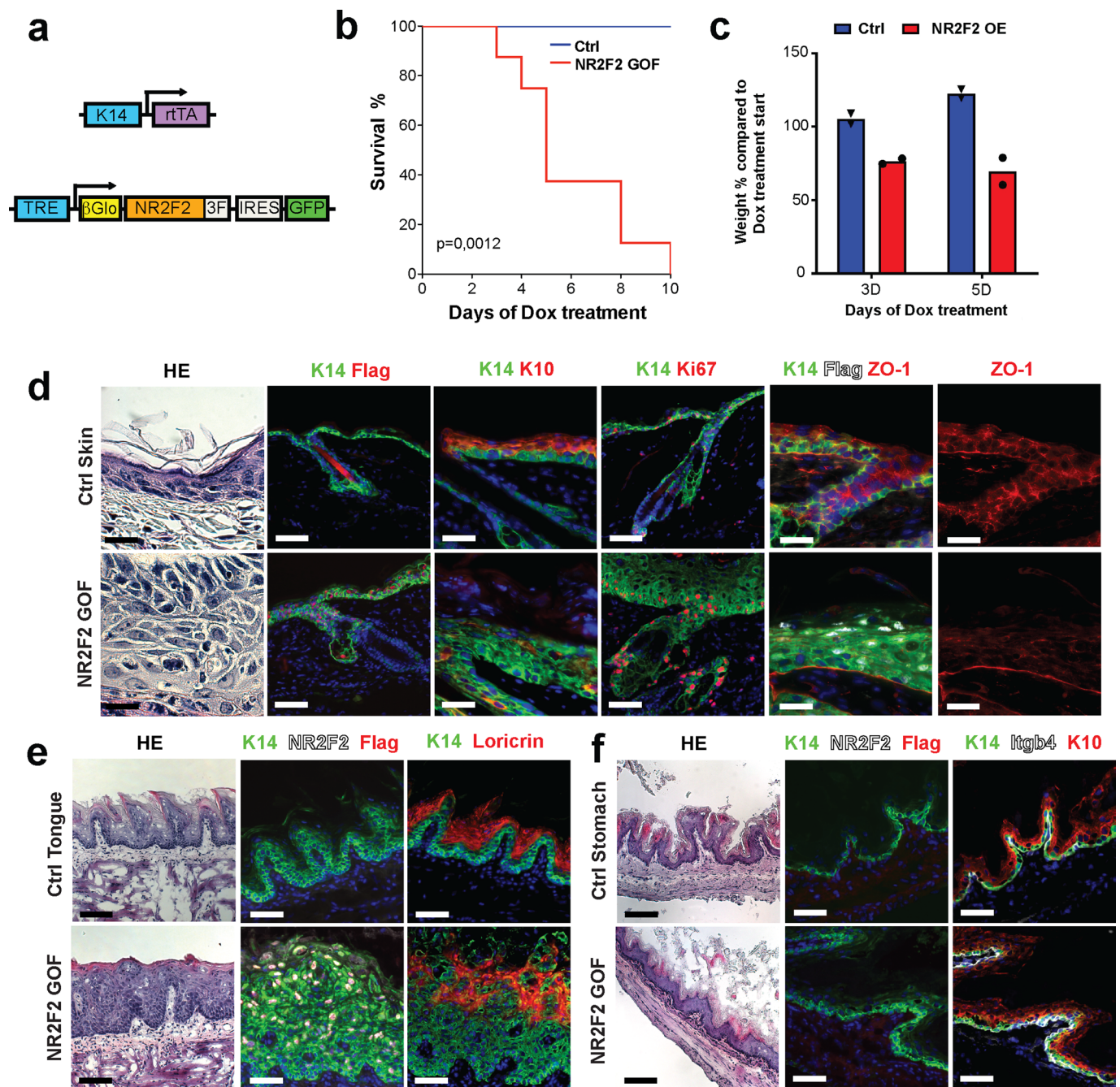
Publisher's note Springer Nature remains neutral with regard to jurisdictional claims in published maps and institutional affiliations.

© The Author(s), under exclusive licence to Springer Nature America, Inc. 2021

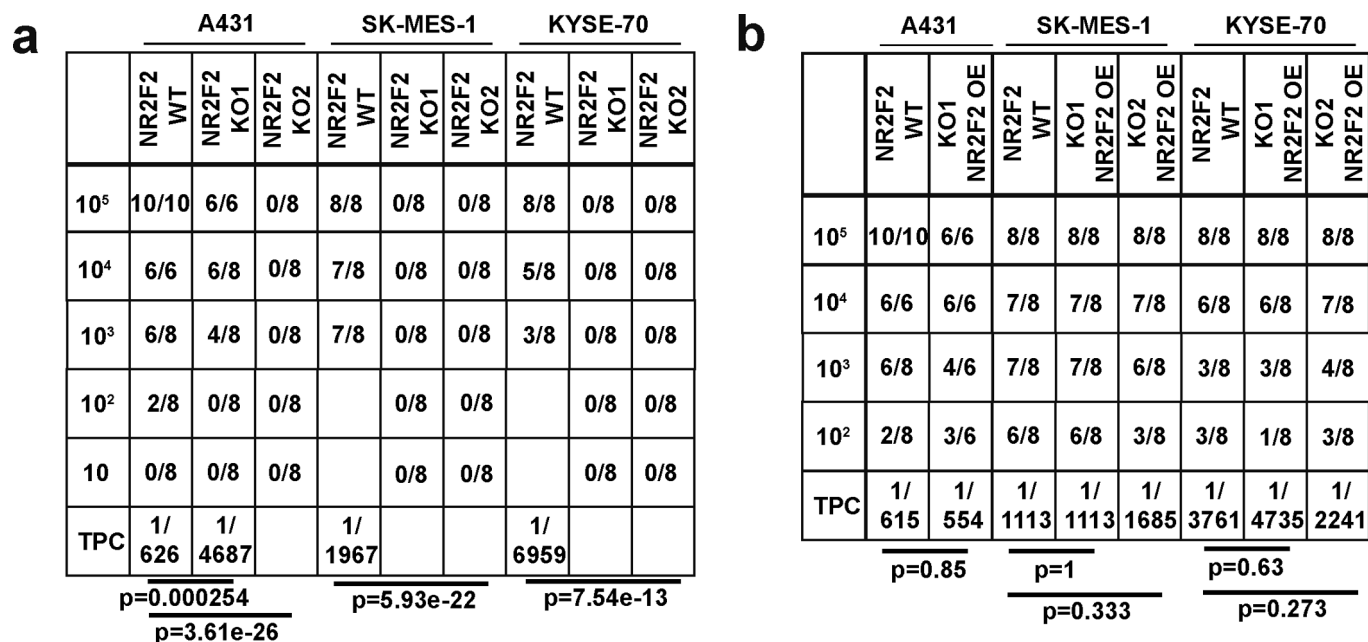


Extended Data Fig. 1 | See next page for caption.

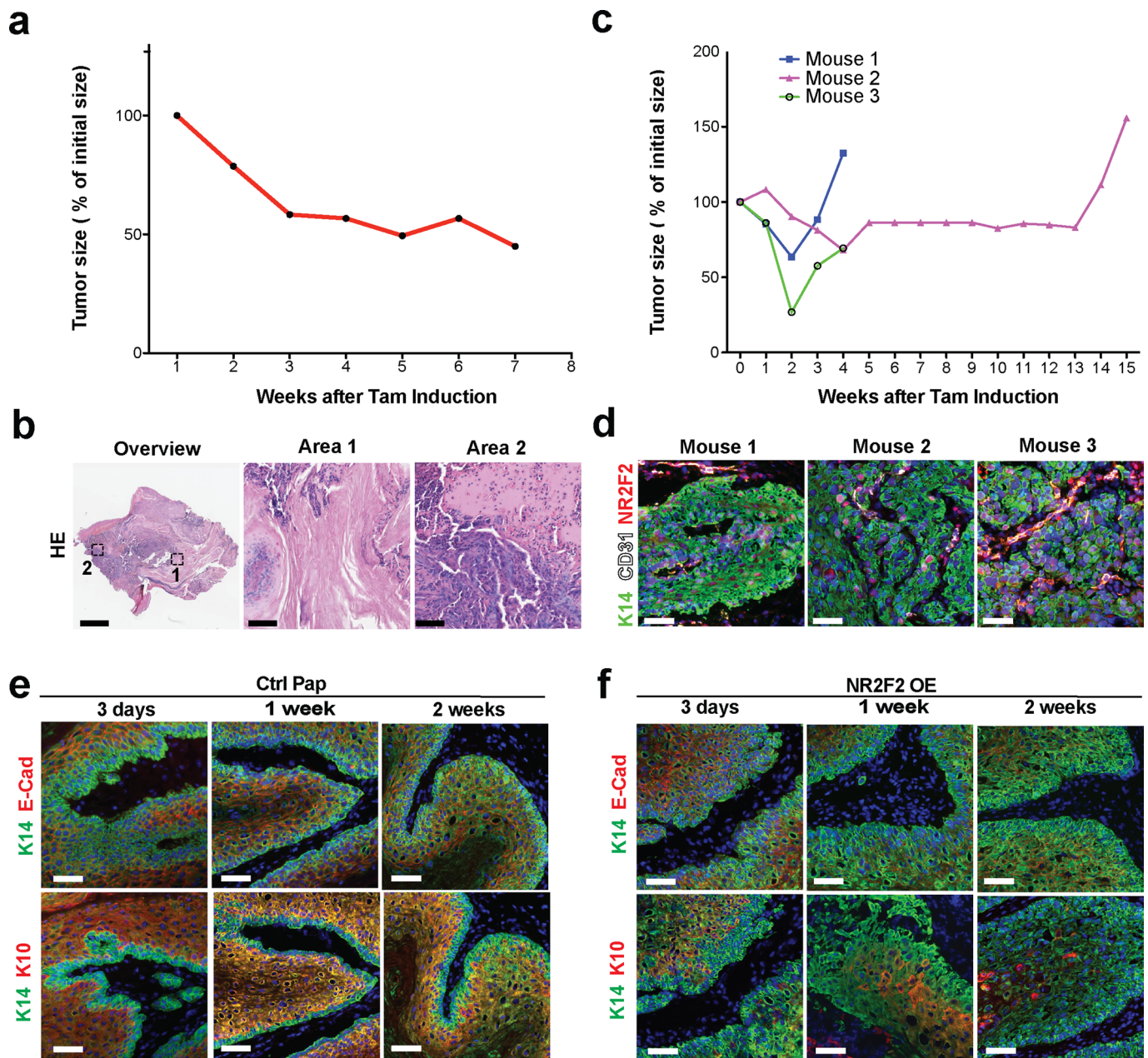
Extended Data Fig. 1 | NR2F2 expression is associated with tumor progression in mouse squamous skin tumors. **a:** Scheme of the strategy used to isolate and transcriptionally profile CSCs from benign papillomas and malignant carcinomas. **b:** Bar graph representation of the relative mRNA expression of the transcription factors that are most highly upregulated in CD34+ cells from mouse malignant carcinoma vs benign papillomas (Fold change CD34+ CSC from carcinoma / papilloma; cells isolated from independent n=4 carcinoma samples and 3 papilloma samples). Data are represented as mean \pm SEM of the ratio between the gene expression level in CD34+ cells in carcinoma samples and the average of all papilloma samples. **c:** Immunostaining for GFP (tumor cells), NR2F2 and Ki67 (proliferating cells) in DMBA SCC. Representative images of minimum 5 independent biological replicates. **d:** Quantification of the percentage of proliferating tumor cells that are positive for NR2F2 expression (n=9 independent tumor samples). **e:** Immunostaining for K14 (Epithelial tumor cells), K10 (differentiating cells) and Itg β 4 (basal membrane), NR2F2 and CD31 (endothelial cells) in papillomas from Ctrl and NR2F2 KO mice (*K14Cre Nr2f2^{fllox}*). Representative images of 5 independent biological replicates. **f:** Immunostaining for K14 (Epithelial cells), YFP (tumor cells) and Vimentin (mesenchymal cells) in differentiated, mixed and mesenchymal genetic tumors (*Igr5CreER/KRas^{G12D}/p53^{fllox}/RosaYFP*). Serial sections from the same tumor samples shown in Fig. 1c. Representative images of minimum 4 independent biological replicates per tumor type. **g:** NR2F2 is necessary for malignant progression in *K14CreER/KRas^{G12D}/p53^{fllox}/RosaYFP*. Number of benign tumors (papillomas) and of malignant SCC per mouse in Ctrl and NR2F2 KO (n=9 Ctrl and 9 NR2F2 KO mice). Scale bar=50 μ m. Data in d and g are represented as mean \pm SEM. The p-values are calculated using a two-tailed Mann-Whitney test.



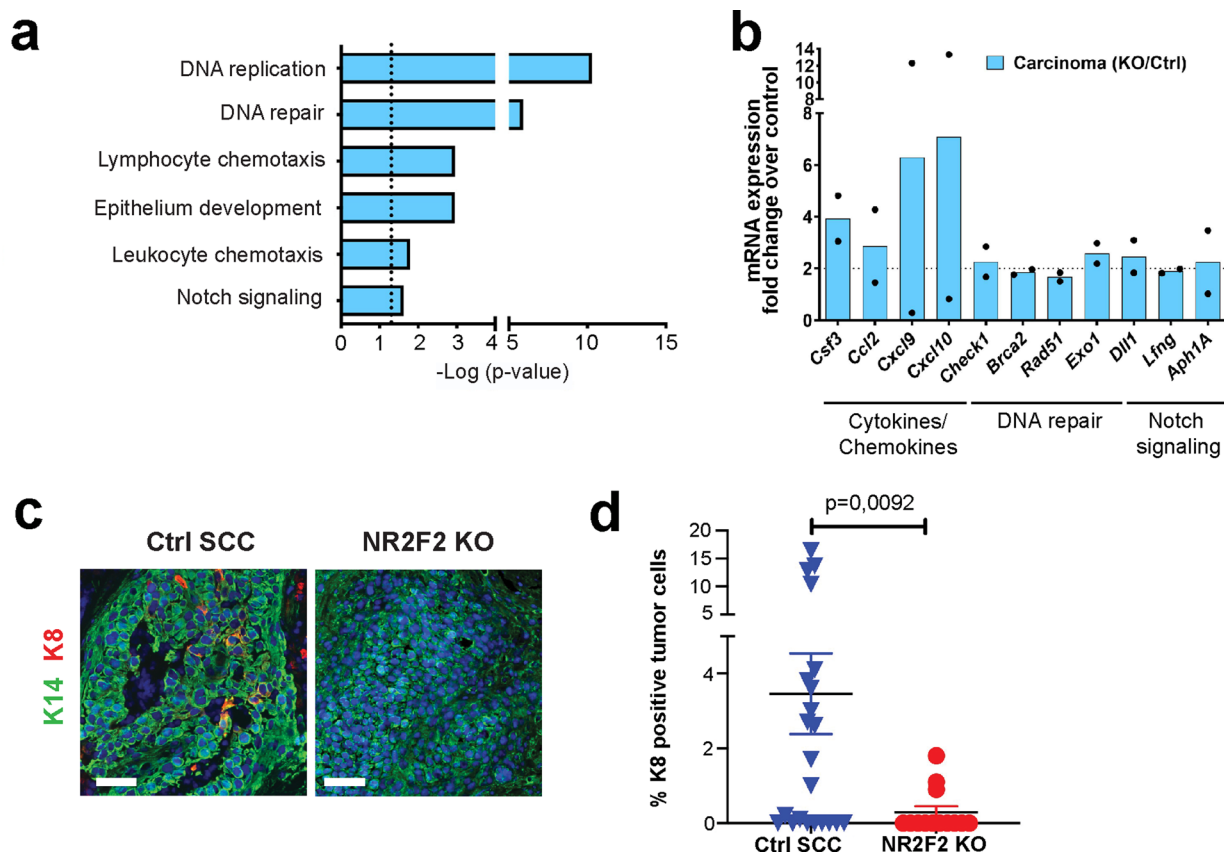
Extended Data Fig. 2 | NR2F2 ectopic expression induces defects of epidermal differentiation. **a-c:** Ectopic NR2F2 expression induces weight loss and death. **a:** Scheme of the transgene allowing Doxycycline inducible expression of NR2F2-3XFlag. **b:** Survival curve of the mice after NR2F2 induction (n=9 mice per genotype). **c:** Graph of the weight of NR2F2 GOF mice and control counterparts after NR2F2 induction (n=2 mice per condition). **d-f:** Ectopic expression of NR2F2 induces defect of epidermal differentiation. **d:** HE and immunostaining for K14, Flag, K10, Ki67 and ZO-1 in mouse skin in NR2F2 GOF and Control. **e:** HE and immunostaining for K14, NR2F2, Flag, and Loricrin in mouse tongue in NR2F2 GOF and Control. **f:** HE and immunostaining for K14, NR2F2, Flag, and Itgb4 in mouse stomach in NR2F2 GOF and Control. Representative images of at least 4 independent biological replicates are shown in d-f. The p-values are calculated using the Long-Rank-Mantel-Cox test in b. Scale bar = 50 μ m.



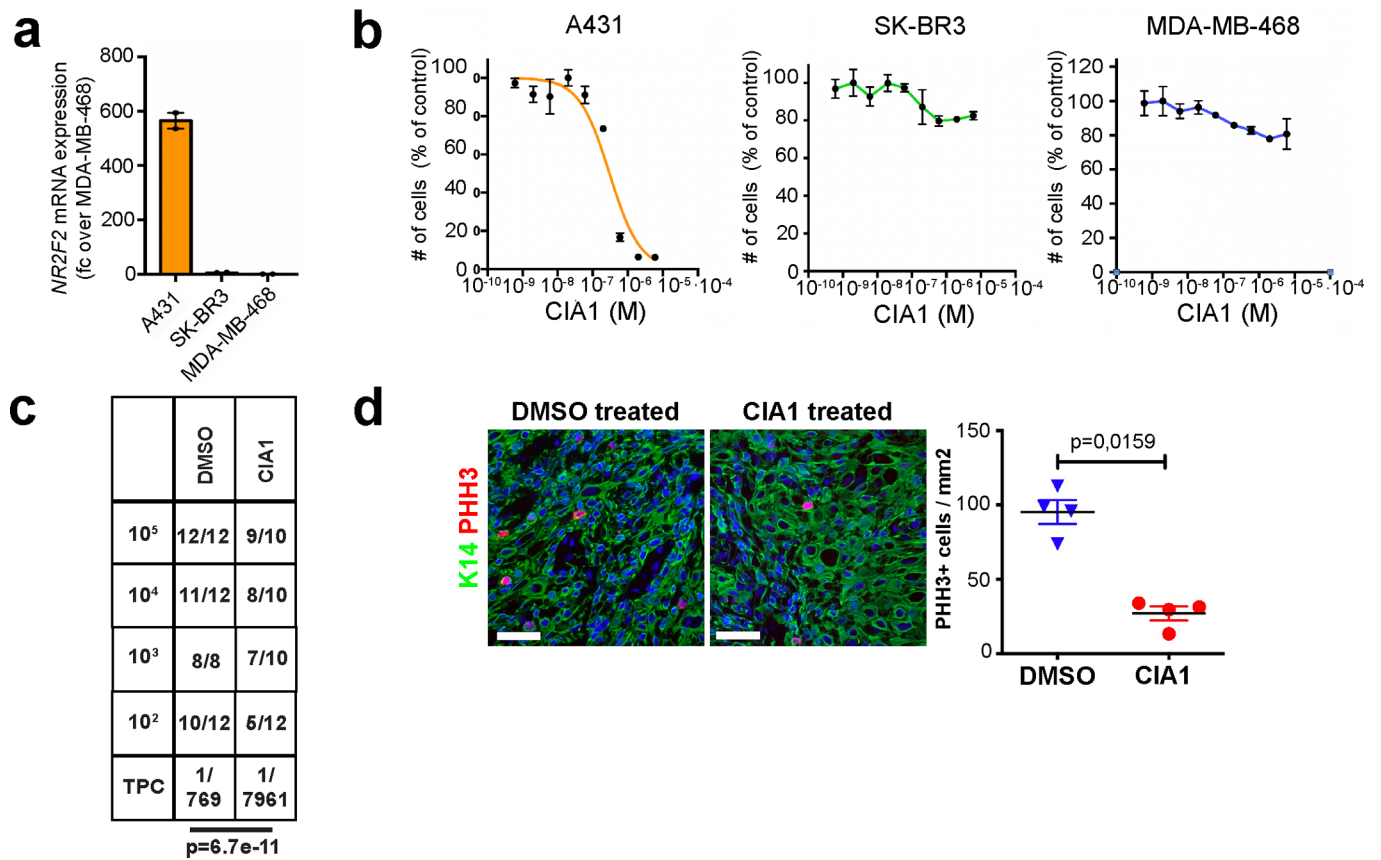
Extended Data Fig. 3 | NR2F2 promotes tumor stemness in human SCC. **a:** Proportion of secondary tumor formation and tumor propagating cell frequency calculated using the extreme limiting dilution analysis (ELDA) for A431 (skin SCC), SK-MES-1(lung SCC) and Kyse-70 (esophagus SCC) WT and NR2F2 KO human SCC cell lines. p-value is calculated using chi-squared test. **b:** Proportion of secondary tumor formation and tumor propagating cell frequency calculated by using the extreme limiting dilution analysis (ELDA) for A431, SK-MES-1 and Kyse-70 parental SCC cell lines and NR2F2 KO rescue clones carrying the NR2F2-3HA transgene. p-value is calculated using chi-squared test.



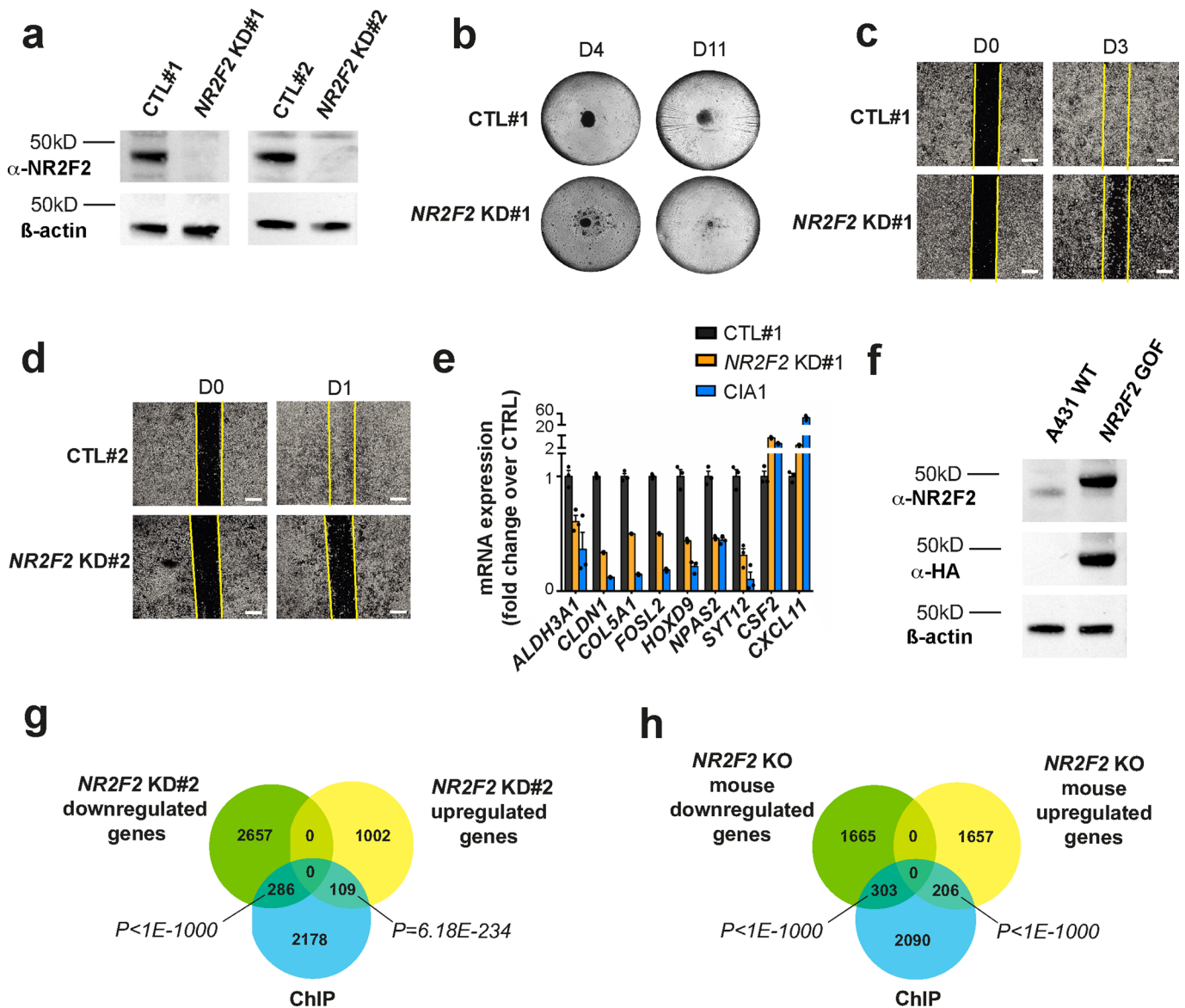
Extended Data Fig. 4 | NR2F2 expression is necessary for malignant tumor maintenance in murine SCC. **a:** Tumor size over time and **b:** HE in NR2F2 KO SCC that reaches a steady size. Higher magnification shows that the residual mass is formed by terminally differentiated cells (Area 1) or necrotic/fibrotic tissue (Area 2). **c:** Tumor size over time and **d:** immunostaining for K14, NR2F2 and CD31 show that relapsing tumors escaped tamoxifen induced *Nr2f2* deletion. **e:** Immunostaining for K14 (epithelial tumor cells), E-Cad (adherens junctions) and K10 (differentiation marker) at 3 days, 1 week and 2 weeks after beginning of doxycycline induction in Ctrl papillomas. **f:** Immunostaining for K14 (epithelial tumor cells), E-Cad (adherens junctions) and K10 (differentiation marker) at 3 days, 1 week and 2 weeks after beginning of doxycycline induction in NR2F2 OE papillomas. Representative images of at least 4 independent biological replicates are shown in e and f. Scale bar = 50 μ m, except overview scale bar = 1mm.



Extended Data Fig. 5 | Downstream changes induced by NR2F2 loss of function in mouse SCC. **a:** Gene ontology analysis of the genes that are upregulated in NR2F2 KO carcinomas, showing categories that are significantly enriched (dotted line $p=0,05$). The p-value is calculated according to the Benjamini-Hochberg method for multiple hypothesis testing. **b:** Bar graph representation of selected genes that are upregulated in NR2F2 KO tumors, grouped by their respective function (Fold change KO/Control; $n=2$ Ctrl and NR2F2 KO carcinomas, independent biological replicates). **c:** Immunostaining for K14 (tumor cells) and K8 (progression marker) in NR2F2 KO and Ctrl SCC. **d:** Quantification of K8 expressing tumor cells in NR2F2 KO and Ctrl SCC ($n=22$ Ctrl and 13 NR2F2 KO tumors). Scale bar = 50 μm . Data in d are represented as mean \pm s.e.m. The p-value is calculated using a two-tailed Mann-Whitney U -test.



Extended Data Fig. 6 | Effects of NR2F2 inhibition in a human skin SCC model. a: Relative expression level of NR2F2 in A431, SK-BR3 and MDA-MB-468 cells (n=2 biological replicates). Data are normalized to MDA-MB-468. Data are represented as mean \pm SEM. **b:** Viability of A431, SK-BR3 and MDA-MB-468 cells 72h after CIA1 treatment *in vitro* (n=3 biological replicates). Data are represented as mean \pm SD. **c:** Proportion of secondary tumor formation and tumor propagating cell frequency calculated by using the extreme limiting dilution analysis (ELDA) of human skin SCC cells (A431) following CIA1 treatment. p-value is calculated using a chi-squared test. **d:** Histology of CIA1 treated xenograft tumors. Immunostaining (left) for PHH3 (mitotic cells) and K14 (Tumor cells) and quantification (right) of PHH3+ cells/mm² (n=4 Ctrl and 4 CIA1 treated tumors). Scale bar = 50 μ m. Data are represented as mean \pm s.e.m. The p-value is calculated using the two-tailed Mann-Whitney U-test.



Extended Data Fig. 7 | NR2F2 loss of function characterization in skin human SCC cell lines. **a:** WB for NR2F2 and β-actin in A431 control and NR2F2 shRNA KD #1 and #2 human cell lines. **b:** NR2F2 knockdown alters the growth of spheroids of A431 skin SCC cell lines. Pictures were taken 4 and 11 days after seeding. Representative images of 3 independent experiments. **c, d:** Wound-healing assay of NR2F2 shRNA KD #1 (c) and #2 (d) following doxycycline induction. Scale bar=500 μm. Representative images of 3 independent experiments. **e:** qRT-PCR of upregulated and downregulated genes following NR2F2 KD and CIA1 exposure in A431 cell line (n=3 technical replicates). Data are represented as mean ± s.e.m. **f:** WB for NR2F2, HA and β-actin in A431 NR2F2 GOF human cell line (A431 WT and 3HA-NR2F2 GOF). **g:** Overlap of the A431 NR2F2 ChIP-seq peaks with the downregulated and upregulated genes in the NR2F2 KD#2 cell line (p-values are calculated using a Two-sided hypergeometric test). **h:** Overlap of the A431 NR2F2 ChIP-seq peaks with the downregulated and upregulated genes in the NR2F2 KO mouse SCC. p-values are calculated using a Two-sided hypergeometric test. WBs are representative of two independent experiments with similar results in f, and three independent experiments with similar results in a.

Reporting Summary

Nature Portfolio wishes to improve the reproducibility of the work that we publish. This form provides structure for consistency and transparency in reporting. For further information on Nature Portfolio policies, see our [Editorial Policies](#) and the [Editorial Policy Checklist](#).

Statistics

For all statistical analyses, confirm that the following items are present in the figure legend, table legend, main text, or Methods section.

n/a Confirmed

- The exact sample size (n) for each experimental group/condition, given as a discrete number and unit of measurement
- A statement on whether measurements were taken from distinct samples or whether the same sample was measured repeatedly
- The statistical test(s) used AND whether they are one- or two-sided
Only common tests should be described solely by name; describe more complex techniques in the Methods section.
- A description of all covariates tested
- A description of any assumptions or corrections, such as tests of normality and adjustment for multiple comparisons
- A full description of the statistical parameters including central tendency (e.g. means) or other basic estimates (e.g. regression coefficient) AND variation (e.g. standard deviation) or associated estimates of uncertainty (e.g. confidence intervals)
- For null hypothesis testing, the test statistic (e.g. F , t , r) with confidence intervals, effect sizes, degrees of freedom and P value noted
Give P values as exact values whenever suitable.
- For Bayesian analysis, information on the choice of priors and Markov chain Monte Carlo settings
- For hierarchical and complex designs, identification of the appropriate level for tests and full reporting of outcomes
- Estimates of effect sizes (e.g. Cohen's d , Pearson's r), indicating how they were calculated

Our web collection on [statistics for biologists](#) contains articles on many of the points above.

Software and code

Policy information about [availability of computer code](#)

Data collection Image acquisition was performed on a Zeiss Axio Imager M1 (Thornwood) fluorescence microscope with a Zeiss Axiocam MR3 camera using the Axiovision software release 4.6. Flow cytometry: FACS ARIA III (for FACS sorting) and FACSDiva software.

Data analysis The quantification of IF and IHC images was performed using ImageJ (<https://imagej.nih.gov/ij/>) and NDP.view2 softwares (<https://www.hamamatsu.com/eu/en/product/type/U12388-01/index.html>). The t-test, Fisher exact test and Anova analysis were performed using Prism (version 8). The RNAsequencing data were analyzed using STAR software (2.4.2a). The gene ontology analysis based on the datasets from the transcriptional profiling of mouse SCC and of human lung SCC cells has been performed using the Enrichr online software. Flow cytometry: FACS ARIA III (for FACS sorting) and FACSDiva software (for FACS data analysis).

For manuscripts utilizing custom algorithms or software that are central to the research but not yet described in published literature, software must be made available to editors and reviewers. We strongly encourage code deposition in a community repository (e.g. GitHub). See the Nature Portfolio [guidelines for submitting code & software](#) for further information.

Data

Policy information about [availability of data](#)

All manuscripts must include a [data availability statement](#). This statement should provide the following information, where applicable:

- Accession codes, unique identifiers, or web links for publicly available datasets
- A description of any restrictions on data availability
- For clinical datasets or third party data, please ensure that the statement adheres to our [policy](#)

All the raw microarray and sequencing data have been deposited in the Gene Expression Omnibus under the following accession codes: GSE164605 (reference series of the whole data), GSE175726 (human RNA-seq), GSE164597 (Microarray carcinoma and papilloma cancer stem cells), GSE164602 (Microarray papilloma)

Field-specific reporting

Please select the one below that is the best fit for your research. If you are not sure, read the appropriate sections before making your selection.

Life sciences Behavioural & social sciences Ecological, evolutionary & environmental sciences

For a reference copy of the document with all sections, see [nature.com/documents/nr-reporting-summary-flat.pdf](https://www.nature.com/documents/nr-reporting-summary-flat.pdf)

Life sciences study design

All studies must disclose on these points even when the disclosure is negative.

Sample size	Samples size for each experiment is indicated in the figures or corresponding figure legends. The sample size was chosen based on previous experience in the laboratory, for each experiment to yield high power to detect specific effects. The previous experiences refers to: the data on the frequency of appearance of tumors and tumor progression in DMBA/TPA and genetic models of skin SCC, tumor cellular and molecular heterogeneity of the different tumor types, the frequency of metastasis, the frequency of secondary tumors upon subcutaneous transplantation and the tumor propagating cell frequency, etc (Pastushenko Nature 2020, Latil Cell Stem Cell 2017, Beck Cell Stem Cell 2015, Boumahdi Nature 2014, Revenco Cell Rep 2019, Lapouge EMBO J 2012). No statistical methods were used to predetermine sample size.
Data exclusions	No data were excluded from the analysis
Replication	All the experiments were performed in at least 3 biologically independent replicates, unless stated otherwise (e.g. RNAseq and ChIPseq experiments). All replicates reported in the manuscript and on which statistics are based are biological replicates. No technical replicates were used for statistical testing. All attempts at replication of the results were successful.
Randomization	For in vivo studies on primary mouse models, animals were chosen based on correct genotypes: requiring 1 (NR2F2); 2 (K14Cre/NR2F2, K5CreER/NR2F2); 3 (Lgr5CreER/Kras/p53, K14CreER/Kras/p53, K19CreER/Kras/NR2F2GOF) or 4 correct alleles (Lgr5CreER/Kras/p53/NR2F2, K14CreER/Kras/p53/NR2F2 and K19CreER/Kras/K14-rtta/NR2F2GOF). Sex-specific differences were minimized by including similar numbers of male and female animals. K14Cre and K5CreER mice were treated with DMBA/TPA at the age of 6-8 weeks after birth and the mice developed tumors in 4-10 months. All mice from the genetic model (Kras/p53 mice) were induced with Tamoxifen at a age 28-35 days after birth, and the mice developed tumours in 2-3 months, thus minimizing the difference in age of different animals used. For the grafting experiments with the NR2F2 overexpression allele, K19CreER/Kras/NR2F2GOF (control) and K19CreER/Kras/K14-rtta/NR2F2GOF (NR2F2 OE) mice of similar age were induced with Tamoxifen at age 35-60 days after birth, and sacrificed. Their skin was then surgically transplanted onto immunodeficient mice, using a skin patch of similar size from control and NR2F2 OE that were grafted contralaterally. Once benign tumors (papillomas) started developing from each skin graft, doxycycline administration was started. Sex-specific differences were minimized by including similar numbers of male and female animals. Each experiment contained animals from at least 3 different litters. In the subcutaneous or intravenous grafting experiments we used NOD/Scid/Il2 mice of similar age and both female and male. For experiments involving cell culture no allocation in groups was needed.
Blinding	Investigators were blinded to mouse genotypes during experiments, for performing sample analysis, imaging and quantification. For experiments with cell lines the researchers were blinded to cell line genotypes or treatment conditions for analysis, imaging and quantification.

Reporting for specific materials, systems and methods

We require information from authors about some types of materials, experimental systems and methods used in many studies. Here, indicate whether each material, system or method listed is relevant to your study. If you are not sure if a list item applies to your research, read the appropriate section before selecting a response.

Materials & experimental systems

n/a	Involved in the study
<input type="checkbox"/>	<input checked="" type="checkbox"/> Antibodies
<input type="checkbox"/>	<input checked="" type="checkbox"/> Eukaryotic cell lines
<input checked="" type="checkbox"/>	<input type="checkbox"/> Palaeontology and archaeology
<input type="checkbox"/>	<input checked="" type="checkbox"/> Animals and other organisms
<input type="checkbox"/>	<input checked="" type="checkbox"/> Human research participants
<input checked="" type="checkbox"/>	<input type="checkbox"/> Clinical data
<input checked="" type="checkbox"/>	<input type="checkbox"/> Dual use research of concern

Methods

n/a	Involved in the study
<input type="checkbox"/>	<input checked="" type="checkbox"/> ChIP-seq
<input type="checkbox"/>	<input checked="" type="checkbox"/> Flow cytometry
<input checked="" type="checkbox"/>	<input type="checkbox"/> MRI-based neuroimaging

Antibodies

Antibodies used

Antibodies used

CD31 PE (BD Bioscience 553373 Clone Mec13.3), CD140a PE (BD Bioscience 12-1401/624049 Clone APAS), Ep-CAM/CD326 APC/Cy7 (Biolegend 118218 Clone G8.8).

For Immunofluorescence and Immunohistochemistry the following antibodies were used: Primary antibodies: anti-GFP (1:500, Abcam ab6673), anti-K14 (1:1000; chicken polyclonal, Thermo Fisher Scientific MA5-11599), anti-Vimentin (1:200, Abcam ab92547 Clone EPR3776), anti-CD45 (1:500, BD Bioscience 553079 Clone 30-F11), anti-E-Cadherin (1:200, ebioscience 14-3249-82 Clone DECMA-1), anti-Zeb1 (1:250, Bethyl laboratories IHC-00419), anti-Zeb2 (1:250, Sigma SAB 3500513), anti-Krt8/18 (1:1000, DSHB TROMA I), anti-Krt10 (1:3000, Covance/IMTEC PRB-159P-0100), anti-Ki67 (1:1000, Abcam ab15580), anti-ZO1 (1:200, Invitrogen 61-7300), anti-Itgb4 (1:1000, BD Bioscience 553745 Clone 346-11A), anti-Ly6G (1:100, Biolegend/IMTEC 127603 Clone 1A8), anti-CD31 (1:200, BD Bioscience 553373 Clone MEC 13.3), anti-NR2F2 (1:1000, Abcam ab64849; for pre-fixed sections in Fig. 1c Abcam ab211776 Clone EPR18442 1:100), anti-pH3 (1:600, Cell Signaling 9701), anti-LamininV (1:1000, Abcam ab14509), anti-Flag (1:1000, Sigma F1804 Clone M2), Loricrin (1:1000, Covance/Eurogentec PRB-145P-0100), BrdU (1:200, Abcam ab6326 Clone BU1/75 ICR1), anti-Itgb4 (1:1000, BD Bioscience 553745 Clone 346-11A), anti-Itgb3 (1:100, BD 562917 Clone 2C9.G2), anti-Alcam (1:1000, R&D FAB1172F), anti-Fibronectin (1:500, Abcam ab2413), anti-Wnt5a (1:200, R&D AF645), anti-Mmp19 (1:200, Novus Biologicals, NBP1-57094), anti-Panycytokeratin (1:200, Abcam ab7753), anti-ku80 (1:200, Abcam ab97433), anti-CD34 (1:100, BD 560230 Clone RAM34).

The following secondary antibodies were used (dilution 1:400): anti-rabbit, anti-rat, anti-goat, antichick, anti-mouse conjugated to rhodamine Red-X (Jackson ImmunoResearch - Cat.#711-295-152; 712-295-153; 705-295-147; 703-295-155; 715-295-151), Alexa Fluor 647 (Jackson ImmunoResearch - Cat.#711-605-152; 712-605-153; 705-605-147; 703-605-155; 715-605-150) or to Alexa Fluor-A488 (Molecular Probes - Cat.#A21206; A21208; A11055; A11039; A21202).

For immunohistochemistry the VECTASTAIN ABC-HRP Kit, Peroxidase (Rabbit IgG) - (PK-4001) has been used (Vector Laboratories).

For Western Blot the following antibodies were used:

anti-bActin (1:3000, Abcam ab8227), anti-NR2F2 (1:500, R&D PP-H7147-00 Clone H7147) and anti-HA (1:1000, Roche/Sigma 11583816001 Clone 12CA5). As secondary antibodies, we used ECL anti-mouse IgG, HRP conjugated (1:3000, Sigma GENA931), and ECL anti-Rabbit IgG, HRP conjugated (1:3000, Sigma GENA9340). As substrate for revelation, we used Western Lightning Plus ECL (Perkin Elmer).

For the ChIP-seq experiments we used an HA tag antibody (Abcam, ab91110)

Validation

All antibodies we used are commercially available and were validated by the provider. We used the protocols and recommendations of the manufacturer only on validated species (mouse or human). To further ensure the specificity of every batch of Abcam ab64849 anti-NR2F2 antibody, and of the more recently developed Abcam ab211776, we validated every batch of antibody by assessing that the induction of NR2F2 conditional deletion in tumor cells (K14-Cre NR2F2flox and K5-CreER NR2F2flox) leads to the disappearance of the signal in tumor cells, while leaving intact the signal in endothelial cells. We also compared the signal of anti-NR2F2 and anti-Flag antibodies in NR2F2 OE papillomas. In addition, we also performed IF of NR2F2 in Crispr-Cas9 KO cells.

Eukaryotic cell lines

Policy information about [cell lines](#)

Cell line source(s)

SK-MES-1 (human lung SCC), A431 (human skin SCC), Kyse-70 (human oesophagus SCC) and HEK293T cells were purchased from the DSMZ-German Collection of Microorganisms and Cell Cultures GmbH.

Authentication

Sk-MES-1 and Sk-MES-1 NR2F2 KO1; A431 and A431 NR2F2 shRNA #1 and #2 cell lines were authenticated by STR profiling at ATCC. Other cell lines were not authenticated.

Mycoplasma contamination

Cells were tested for mycoplasma as regularly as possible using several available commercial methods (e.g. MycoAlertTM Mycoplasma Detection Kit, Lonza; PCR Mycoplasma Detection Kit, ABM). If mycoplasma contamination was detected, we treated the cells with Plasmocyn treatment/prophylactic (Invivogen) or we discarded them.

Commonly misidentified lines
(See [ICLAC](#) register)

None of the cell lines used are listed in the database of commonly misidentified cell lines maintained by ICLAC.

Animals and other organisms

Policy information about [studies involving animals](#); [ARRIVE guidelines](#) recommended for reporting animal research

Laboratory animals

All the animals used were grown in mixed background. Sex-specific differences were minimized by including similar numbers of male and female animals in all cases.

K14Cre/NR2F2, K14CreER/NR2F2, K5CreER/NR2F2 mice were treated 3 times with DMBA 6-8 weeks after birth and after received treatment with DMBA and TPA once a week until the tumors appeared, switching then to TPA treatment twice a week.

Lgr5CreER/Kras/p53, K14CreER/Kras/p53, Lgr5CreER/Kras/p53/NR2F2 and K14CreER/Kras/p53/NR2F2 mice were induced with Tamoxifen at 28-35 days after birth.

The mice were sacrificed if tumour reached the limit size as described according to ethical protocol or if mice presented signs of distress or weight loss >20% was observed. The average weight of the mice used was 35g (range from 22 to 48g).

For grafting experiments NOD/SCID mice were used with age ranging from 4 to 8 weeks. Both male and female mice were used for these experiments. The weight of these mice was in average 29 g (ranging from 21 to 37g).

NOD/SCID/Il2Ry null mice were used for transplantation and metastasis assays (by performing intravenous grafting of tumor cells).

The housing conditions of all animals were strictly following the ethical regulations. The room temperature ranged from 20 and 25°C. The relative ambient humidity at the level of mouse cages was 55 per cent +/-15. Each cage was provided with food, water and two types of nesting material. Semi-natural light cycle of 12:12 was used.

Wild animals	No wild animals were used in this study.
Field-collected samples	No field-collected samples were used in this study.
Ethics oversight	Mouse colonies were maintained in a certified animal facility in accordance with the European guidelines. All the experiments were approved by the corresponding ethical committee (Commission d'éthique et du bien être animal CEBEA, Faculty of Medicine, Université Libre de Bruxelles). CEBEA follows the European Convention for the Protection of Vertebrate Animals used for Experimental and other Scientific Purposes (ETS No.123). The project proposal was submitted to the Ethical Committee for Animal Experimentation and evaluation and approval. The committee consists of internal and external members with expertise regarding ethics, alternative methods to animal experiments, animal health and welfare as well as research techniques, experimental design and statistical analysis. The ULB ERASME Ethical Committee for Animal Experimentation is responsible for evaluating and approving or rejecting all projects involving animal experiments, as an independent body under Belgian legislation (Royal Decree regarding the protection of laboratory animals of 29 May, 2013) and European directive (2010/63/EU). For every project proposal, the Ethical Committee for Animal Experimentation takes the so-called 3R principle (see Replacing, Reducing, Refining) as its guiding principle and in accordance with the European Guidelines. The project authorization was approved under the number 665N from the ULB ERASME Ethical Committee for Animal Experimentation. The mice were checked every day and were euthanized when the tumor reach the end-point size (1 cm in diameter for all experiments; 2 cm in diameter for the experiments described in Fig. 7e) or if the tumor was ulcerated independently of its size, if the mouse lost >20% of the initial weight or any other sign of distress appeared (based on the general health status and spontaneous activity). None of the experiments performed in this study surpassed the size limit of the tumors. All the experiments strictly complied with the protocols approved by the ethical committee.

Note that full information on the approval of the study protocol must also be provided in the manuscript.

Human research participants

Policy information about [studies involving human research participants](#)

Population characteristics	Adult patients with head and neck, skin, lung, esophagus SCC, actinic keratosis. The researchers involved in this work did not have access to the clinical data (such as age or gender). All the samples received were assigned by the clinician or surgeon responsible for patient care a unique code.
Recruitment	<p>The samples were provided by Erasme Biobank and originate from adult patients that developed head and neck, lung, skin or esophagus SCC or actinic keratosis, as well as the corresponding normal skin controls. The analyzed samples were harvested from the surgically removed material, not directly from patients. All the samples belong to the Erasme Biobank(B406201525681).</p> <p>Concerning SCC, only primary tumors or recurrent tumors from the 4 pre-described sites were studied. There was no restriction of age (except that only adult patients were included) or gender, and no pre-treated tumors were included.</p> <p>The goal of the study was to examine the expression and the localization of NR2F2 in different contexts. There was no intention of correlation with histopathology tumor grade or tumor aggressiveness.</p>
Ethics oversight	The human collection study was approved by the Erasme ethical committee. Reference: P2015/330 / /B406201525681.

Note that full information on the approval of the study protocol must also be provided in the manuscript.

ChIP-seq

Data deposition

- Confirm that both raw and final processed data have been deposited in a public database such as [GEO](#).
- Confirm that you have deposited or provided access to graph files (e.g. BED files) for the called peaks.

Data access links <i>May remain private before publication.</i>	GSE175724
Files in database submission	.fastq and .bed files relative to 2 independent input samples and two independent ChIP samples (total 4 .fastq files in total (2x input and 2x IP) and 2 .bed files.
Genome browser session (e.g. UCSC)	https://genome.ucsc.edu/s/Yura%20SONG/hg38%2Dchip%2Dnr2f2

Methodology

Replicates	2 independent biological replicates from inducible A431 NR2F2-GOF cell line (2x input and 2x ChIP).
Sequencing depth	Total number of reads on Input is 35M and that of ChIP is 120M. Number of uniquely mapped read: input 21M, ChIP 71M. Paired reads of 100bp length.
Antibodies	Anti-HA tag antibody (Abcam, ab91110).

Peak calling parameters	Peak calling parameters: -f BAMPE -g hs -p 0.01 --nomodel
Data quality	In FDR 1%, the number of peaks is 17699.
Software	<p>Before starting the alignment and downstream analysis, quality check was done by FastQC (https://www.bioinformatics.babraham.ac.uk/projects/fastqc/). The alignment and peak calling were managed on Consortium des Équipements de Calcul Intensif (CÉCI). Adaptors sequences and low-quality regions were removed with Trimmomatic (ver 1.11) paired-end mode using options "HEADCROP:10 CROP:65 ILLUMINA_CLIP:adaptor.file:2:30:10 LEADING:3 TRAILING:3 SLIDINGWINDOW:4:15 MINLEN:50". Trimmed reads were then aligned to human reference genome hg38 using Bowtie2 (version 2.3.4.2) using options "-X 2000 -q -p 6 -t --fr --very-sensitive --no-discordant --no-unal --no-mixed". Mitochondrial reads, reads from unmapped and random contigs, reads without unique alignment, reads with a mapping quality less than 20 and reads which are not properly mapped were removed using samtools (version 1.11). Duplicate reads were removed by Picard MarkDuplicates (http://broadinstitute.github.io/picard/). Peak calling was performed by macs2 (version 2.2.5) using options "-f BAMPE -g hs -p 0.01 --nomodel". Blacklisted regions are filtered out by bedtools intersect (version 2.27.1).</p> <p>The raw count was globally normalized into count per 1 million. Peaks were associated to genes with GREAT software (version 4.0.4) with the following parameters: 5.0kb in proximal upstream, 1.0kb in proximal downstream and up to 100.0kb in distal.</p> <p>De novo motif prediction was performed using findMotifsGenome.pl program in HOMER (version 4.10) software using parameters "-size -250,250 -S 15 -len 6,8,10,12."</p>

Flow Cytometry

Plots

Confirm that:

- The axis labels state the marker and fluorochrome used (e.g. CD4-FITC).
- The axis scales are clearly visible. Include numbers along axes only for bottom left plot of group (a 'group' is an analysis of identical markers).
- All plots are contour plots with outliers or pseudocolor plots.
- A numerical value for number of cells or percentage (with statistics) is provided.

Methodology

Sample preparation	Skin tumors from DMBA/TPA treated mice, Lgr5CreER/Kras/p53/NR2F2, K14CreER/Kras/p53/NR2F2 and K19CreER/Kras/K14rtta/NR2F2 GOF mice were dissected, minced and digested in Collagenase type I (Sigma) at 3.5 mg/ml during 1 hour at 37°C on a rocking plate. Collagenase activity was blocked with by the addition of EDTA (5mM) and then the cells were rinsed in PBS supplemented with 2% FBS and the cell suspensions were filtered through a 70um cell strainers (BD). For in vitro experiments (AldeFluor), cells were processed according to the manufacturer's instructions.
Instrument	FACSAria and LSRFortessa (BD Bioscience)
Software	FACSDiva and FACSAria Software (BD Bioscience)
Cell population abundance	The proportion of Epcam+ tumor cells in the viable population varied from 5 to 40%. The proportion of tumor cell subpopulations within tumor cells varied depending on the tumor type and between individual tumors.
Gating strategy	Living cells were selected by forward scatter, side scatter, doublets discrimination and by Hoechst dye exclusion. Epithelial tumor cell subpopulations were selected based on the expression of Epcam and the exclusion of CD140a, CD45 and CD31. For the experiment described in Fig. 1D, Epcam positive and negative tumor cells were selected based on the expression of YFP and the exclusion of CD45 and CD31.

- Tick this box to confirm that a figure exemplifying the gating strategy is provided in the Supplementary Information.